The Western North Atlantic Shelfbreak Current System in Summer

PAULA S. FRATANTONI AND ROBERT S. PICKART

Department of Physical Oceanography, Woods Hole Oceanographic Institution, Woods Hole, Massachusetts

(Manuscript received 18 March 2005, in final form 10 January 2007)

ABSTRACT

Twelve years of historical hydrographic data, spanning the period 1990–2001, are analyzed to examine the along-stream evolution of the western North Atlantic Ocean shelfbreak front and current, following its path between the west coast of Greenland and the Middle Atlantic Bight. Over 700 synoptic sections are used to construct a mean three-dimensional description of the summer shelfbreak front and to quantify the along-stream evolution in properties, including frontal strength and grounding position. Results show that there are actually two fronts in the northern part of the domain—a shallow front located near the shelf break and a deeper front centered in the core of Irminger Water over the upper slope. The properties of the deeper Irminger front erode gradually to the south, and the front disappears entirely near the Grand Banks of Newfoundland. The shallow shelfbreak front is identifiable throughout the domain, and its properties exhibit large variations from north to south, with the largest changes occurring near the Tail of the Grand Banks. Despite these structural changes, and large variations in topography, the foot of the shelfbreak front remains within 20 km of the shelf break. The hydrographic sections are also used to examine the evolution of the baroclinic velocity field and its associated volume transport. The baroclinic velocity structure consists of a single velocity core that is stronger and penetrates deeper where the Irminger front is present. The baroclinic volume transport decreases by equal amounts at the southern end of the Labrador Shelf and at the Tail of the Grand Banks. Overall, the results suggest that the Grand Banks is a geographically critical location in the North Atlantic shelfbreak system.

1. Introduction

The coastal circulation in the western North Atlantic Ocean is dominated by the equatorward flow of subpolar and Arctic-origin water. The export of freshwater through Denmark Strait and Davis Strait, and the accumulation of coastal discharge along the length of the subpolar continental shelf, establish a thermohaline front that separates relatively cold, fresh shelf waters from warm, salty waters on the continental slope. The shelf/slope front, generally centered near the shelf break (hence also referred to as the shelfbreak front), supports a persistent, surface-intensified current. Progressing from north to south this shelfbreak current has many regional names (Fig. 1), but to some degree it is a single large-scale feature.

The shelfbreak current originates as the East Greenland Current flowing out of Denmark Strait, advecting Arctic-origin waters out of the Nordic seas (e.g., Rudels et al. 2002; Fig. 1). South of Denmark Strait, the East Greenland Current is joined by the retroflecting Irminger Current, carrying Gulf Stream–remnant water over the upper Greenland slope (Buch 2000). The Irminger Current and East Greenland Currents are typically depicted as two distinct features, flowing side-by-side in schematic circulation diagrams. The diagrams often show the Irminger Current disappearing at the southern tip of Greenland while the East Greenland Current rounds Cape Farewell and flows northward as the West Greenland Current. More accurately, the East Greenland and Irminger Currents may be thought of as a merged current system, indistinguishable in velocity (Pickart et al. 2005), but identifiable in hydrographic properties (e.g., Clarke 1984).

After rounding the southern tip of Greenland, the West Greenland Current continues northward along the shelf break, transporting relatively cold, fresh water along the outer shelf and warm, salty "Irminger Sea water" over the slope. Just south of Davis Strait the flow bifurcates: part of the current turns westward to flow cyclonically around the Labrador basin, and the

Corresponding author address: Paula S. Fratantoni, Department of Physical Oceanography, Woods Hole Oceanographic Institution, Woods Hole, MA 02543.
E-mail: pfratantoni@whoi.edu

DOI: 10.1175/JPO3123.1

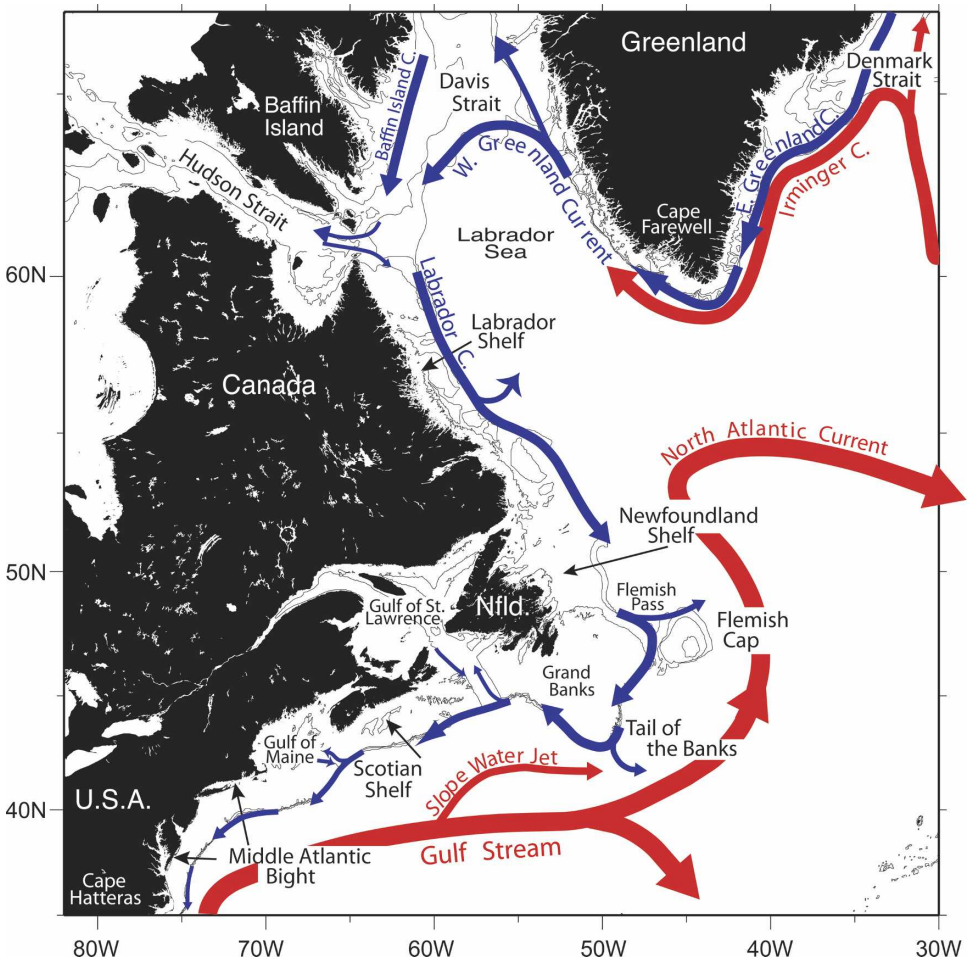

FIG. 1. Schematic diagram depicting major features of the surface circulation in the western North Atlantic. The path of the shelfbreak jet is designated by blue arrows while the warmer, Gulf Stream–origin currents are drawn in red.

remainder continues northward into Baffin Bay. This splitting was first documented long ago and has been noted by many authors, but the precise division of transport has not yet been quantified. It is commonly believed that the majority of the current turns westward (e.g., Baggesgaard-Rasumssen and Jacobsen 1930; Cuny et al. 2002; Reverdin et al. 2003).

Upon reaching the edge of the Labrador shelf, the current turns southward and is joined by the Baffin Island Current (Smith et al. 1937) exiting Davis Strait and by outflow from Hudson Strait. This combined flow is referred to as the main branch of the Labrador Current[1] (Lazier and Wright 1993), which continues southward through Flemish Pass and around the Grand Banks of Newfoundland. At the Tail of the Banks, the shelfbreak current undergoes a second major bifurcation. Part of the Labrador Current recirculates to the east, inshore of the North Atlantic Current (Clarke et al. 1980), while the remainder continues equatorward (Fig. 1). The exact degree of this division is not known, but it is generally thought that most of the flow recirculates eastward (Loder et al. 1998). In any event, it is a time-dependent process that varies on both interannual and seasonal time scales (e.g., Petrie and Drinkwater 1993). West of the Grand Banks the remaining portion of the shelfbreak current continues equatorward along the edge of the Scotian shelf and into the Middle Atlantic Bight (MAB), terminating inshore of the Gulf Stream off Cape Hatteras, North Carolina.

Over the years many studies have addressed different

[1] This is to be distinguished from the "barotropic" branch of the Labrador Current, which resides farther offshore over the deep continental slope and carries the bulk of the Sverdrup return flow of the subpolar gyre (Lazier and Wright 1993).

aspects of the western North Atlantic shelfbreak current system. Most of these studies have been regional, focusing on a particular segment of the current. While the locus of such efforts has greatly advanced our understanding of the shelfbreak current, we are still lacking an overall understanding of the large-scale nature of the system. For instance, the surface expression of the front is found well offshore of the shelf break in some places (Loder et al. 1998), yet at others it appears to be tied to the shelfbreak (Wright 1976). Observations also indicate that the velocity structure of the current is quite varied in different geographical regions—for instance, the deep-reaching West Greenland Current (Smith et al. 1937; Lazier 1980) versus the relatively shallow jet of the MAB (Fratantoni et al. 2001). Finally, it is known that the current experiences a substantial decrease in volume transport from north to south (Loder et al. 1998). However, it has not been determined if most of the transport loss occurs at a small number of discrete locations (e.g., the two bifurcation areas noted above), or if there is a continual transport loss along the full length of the current (or both). In general, the along-stream evolution and/or continuity in structure, properties, transport, and cross-shelf location of the jet and front have not yet been quantified.

In this study, we analyze 12 years (1990–2001) of historical hydrographic data to examine the along-stream evolution of the western North Atlantic shelfbreak front and jet during the summer season, following its path from Cape Farewell, Greenland, to its termination near Cape Hatteras, North Carolina. The overall goal is to quantify the large-scale evolution of the structure, properties, and cross-shelf position of the front and jet over this 6000-km distance. In other words, we aim to investigate the "global" nature of the shelfbreak system. To preserve as much of the three-dimensional structure of the front as possible and to maximize the resolution of the historical observations, we take the unique approach of working with synoptic sections rather than spatially binning and averaging the data. While this is more difficult and time consuming than constructing a typical climatology, it results in a more realistic depiction of this complex system.

We begin with a description of the climatological dataset and outline our methods for computing average hydrographic sections from the data. Next we present a mean three-dimensional description of the shelfbreak front, relating the spatial variability to changes in the baroclinic structure and volume transport of the jet. Last, we quantify the along-stream evolution of frontal properties, including its strength and grounding position.

2. Data and methods

The historical data used in this study comes from the Bedford Institute of Oceanography (BIO) Climate Database (Petrie et al. 1996). The database encompasses the northwestern Atlantic, covering an area roughly bounded by 35°–80°N, 42°–100°W and includes hydrographic profiles collected between 1910 and the present. The climatology includes data from a variety of sources, including bottle stations, conductivity–temperature–depth (CTD) casts, and Batfish[2] measurements extracted from the Canadian Marine Environmental Data Service (MEDS) and the U.S. National Oceanographic Data Center (NODC). For this analysis we examined a 12-yr subset of the historical data collected between 1990 and 2001.

We have chosen Cape Farewell (southern tip of Greenland) as the northern boundary of our domain and Cape Hatteras (where the current ends) as our southern boundary. This distance covers regions with substantially different topography, so we split the domain into 19 boxes, each box corresponding to a fairly distinct topographical regime (Fig. 2). The historical data within each box were used to construct a mean section of the front and jet. It is most common when constructing climatologies to spatially bin and average the data without regard to the synopticity of the measurements. However, this can sometimes lead to noisy fields that are difficult to interpret, especially when the data are relatively sparse (see Pickart 2004). Therefore, in an effort to maximize the spatial resolution of the available data, while best preserving the structure of the front within each regional box, we have taken a different approach. We have identified all of the synoptic sections within each regional box and interpolated each one onto a standard grid, prior to computing regional averages. A similar method was applied successfully to analyze historical data at the shelf break in the western Arctic Ocean (Pickart 2004).

The boundaries of the 19 regional boxes were chosen so that the depth of the shelf break and steepness of the continental slope remain somewhat constant within each area. This allowed us to construct a representative (average) cross-stream bottom profile and corresponding standard grid for each region. Specifically, we aligned the collection of vertical sections within a box relative to the representative topographic profile so that cross-stream distances are measured relative to the location of the shelf break. Individual sections were mapped onto the standard grid by assigning a

[2] A towed undulating CTD.

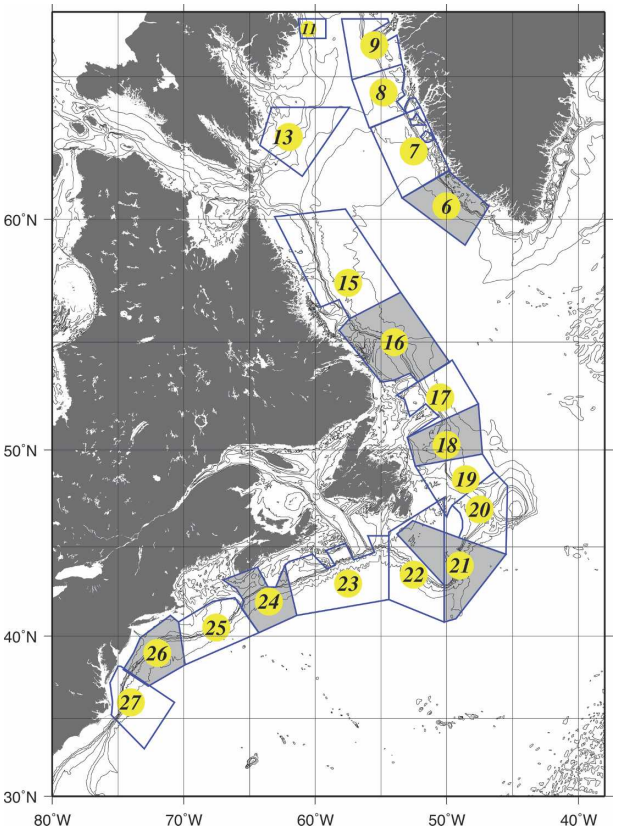

FIG. 2. Map of the study domain showing the location of regional boxes. The mean sections in Fig. 4 were computed from observations in the gray-shaded boxes.

cross-stream position to the corresponding water depth of each hydrographic station (see appendix). Once the projection of the station data was complete, each section was objectively interpolated onto a final grid using a Laplacian-spline objective interpolation scheme. The grid spacing of the final grid is $dx = 5$ km and $dz = 10$ m.

While the method that we have developed to map synoptic sections onto a standard grid allows us to preserve the structure of the front and quantify its variability over this vast domain, it also introduces several limitations to our climatology. For instance, because the water depth of a station is used to determine its cross-shelf position in the regional grid, there can only be one cross-shelf position associated with each water depth. As a result, flat shelves, canyons, and isolated plateaus and basins, all typical features along the continental shelf, lead to spurious mappings and we are unable to map stations near them. Hence, we are not able to capture the rich topographic variability and resulting circulation patterns that often delineate one shelf region from another (e.g., the branching of the Labrador Current on the northeast Newfoundland shelf; Smith et al. 1937). Nonetheless, the simplifications imposed by the standard grid do not detract from, but instead facilitate, our analysis at the shelf break. The reader is referred to the appendix for more details on the construction of the standard grids, for a discussion of issues associated with the projection of the station data, and for specifics about the interpolation and quality control of the data.

The climatology of synoptic sections

The geographic distribution of the final climatology of synoptic sections is shown in Fig. 3. There were a total of 1153 sections in the study region with the majority of sections concentrated in boxes 15–27, along the east coast of North America (Fig. 3, inset). The sections extend as far offshore as the 4000-m isobath, but the majority of the sections terminate between the 200-m and 1500-m isobaths. The sections were divided into winter (October–March), of which there were 451 sections, and summer (April–September), of which there were 702 sections. For this study we consider only the summer sections. Our definition of summer was chosen to coincide with the seasonal stratification that takes place over most of the shelfbreak region. The summer stratification is characterized by the formation of a warm, near-surface layer and by freshening of shelf waters following the spring maximum in coastal runoff and ice melt (Loder et al. 1998). The amplitude and phase associated with this annual cycle varies from region to region (e.g., dependent on the distance to freshwater sources), but the general pattern is consistent throughout the shelfbreak domain. It should be noted that the northern half of the domain is seasonally ice covered for a portion of our "summer" period (April–June), potentially underestimating the summer thermal stratification in this portion of the domain.

The goal of projecting the synoptic observations onto a standard grid was to compute a mean shelfbreak section for each regional box and then to characterize the variability in a quantitative fashion. In general, the data density within each regional box decreases near the edges of the grid. Therefore, a threshold was set for each regional box (Table 1) so that only the portion of the domain containing this number of observations was considered in the subsequent calculations. The value was chosen so that a significant number of observations contribute to the mean while avoiding regions with large gradients in data density, which can result in artificial gradients in the mean fields. Since no summer sections were identified in box 13 and only three were

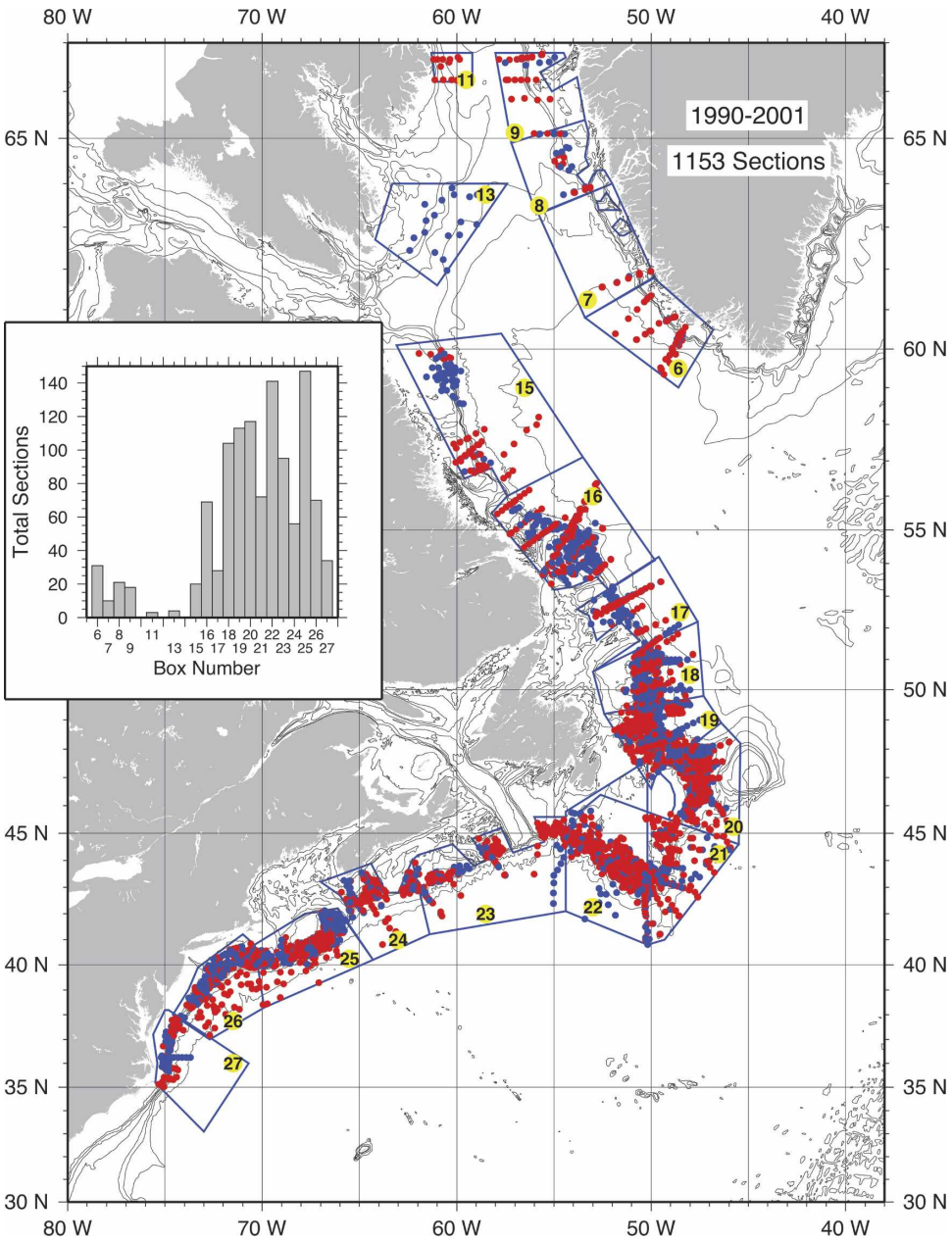

FIG. 3. Geographic distribution of the final climatology of synoptic sections. The red dots are observations collected during summer (April–September) while the blue dots are stations occupied during winter (October–March). A histogram of the number of sections per regional box is shown in the inset.

found in box 11, these regions (the western part of Davis Strait) were excluded from the analysis.

3. Mean sections

Average sections of potential temperature, salinity, and potential density were computed for each of the regional boxes. A subset of these mean sections is shown in Fig. 4 and will be used to illustrate the downstream evolution of properties of the North Atlantic shelfbreak front and jet. We first describe the northern region (upstream of Flemish Cap, Fig. 4a) and then compare these with the southern region (Fig. 4b). The reader should note that the color scales are different in Figs. 4a and 4b in order to accommodate the large difference in temperature and salinity between the northern and southern regions of the domain. For ease of comparison, all sections are plotted on the same scale,

TABLE 1. Spatial coverage of sections within each regional box. The columns correspond to 1) the regional box number in Fig. 2, 2) the total number of sections, 3) the water depth at the seawardmost station, 4) the depth of the deepest observation, 5) the cross-shelf width of the section, and 6) the threshold number of sections required to compute a mean.

Box	No. of sections	Offshore isobath (m)	Deepest observation depth (m)	Cross-shelf width (km)	Threshold
6	23	3405	840	190	10
7	9	3029	1030	175	5
8	11	1520	920	210	6
9	15	590	350	50	8
11	3	—	—	—	—
15	10	2203	500	100	4
16	33	3369	840	240	10
17	17	3442	990	165	6
18	56	2202	880	130	10
19	76	1683	500	160	10
20	79	1464	800	115	10
21	47	3505	1080	165	10
22	95	2165	580	80	10
23	63	3235	810	95	10
24	41	3914	430	185	4
25	71	1673	200	60	10
26	38	3489	330	220	4
27	15	2244	820	70	4

where $x = 0$ corresponds to the location of the shelf break.

a. Northern boxes

As discussed above, the West Greenland Current downstream of Cape Farewell advects a combination of cold, fresh Arctic-origin water and warm, salty Irminger Water (Gulf Stream-remnant water). These two water masses are clearly seen in each of the northern boxes (Fig. 4a; labeled AW and IW, respectively). In particular, the potential temperature sections show a subsurface temperature maximum located over the upper slope, near 400 m, and a corresponding subsurface salinity maximum, although the salinity core is situated slightly deeper than that of the temperature maximum. The warmest and saltiest water is found on the West Greenland shelf (box 6), with temperatures reaching 4.3°C and salinity as high as 34.9 psu. These values are consistent with the properties of Irminger Water (Lazier 1973). Progressing downstream, the gradual erosion of the Irminger Water signal is evident as the subsurface temperature maximum cools by 0.85°C and the subsurface salinity maximum freshens by 0.06 on the Labrador shelf (box 16), disappearing altogether by the Newfoundland shelf (box 18). These changes compare well with the observations of Cuny et al. (2002), who suggest that the cooling and freshening of Irminger Water between the west coast of Greenland and the Labrador shelf result in part from isopycnal mixing with the cold, fresh outflow from Baffin Bay. It is also possible for Irminger Water to be cooled and freshened via wintertime convection in the boundary current in the Labrador Sea (e.g., Pickart et al. 2002). However, our average sections are constructed from more than 12 years of observations, including both strongly convective and weakly convective periods. Therefore, it is more likely that the cooling and freshening of the Irminger Water is accomplished predominantly by isopycnal mixing (see section 5a), with perhaps a contribution from double-diffusive mixing.

By contrast, the water over the shelf in the northern boxes is much colder and fresher, with temperatures as low as −1.3°C and salinities less than 33.5 psu (Fig. 4a). These values are consistent with the properties of water originating in the Nordic seas, Baffin Bay, and Hudson Strait (Lazier and Wright 1993; Cuny et al. 2002). Details of the distribution of temperature and salinity over the shelf are clearer in the θ–S curves shown in Fig. 5a. In the northern boxes, the shelf water reaches a minimum temperature on the Labrador shelf at a salinity of 32.95 psu (Fig. 5a). The coldest water over the shelf ranges from −1.0°C on the Greenland shelf to −1.3°C on the Labrador shelf and −0.4°C on the Newfoundland shelf. This cold water is a remnant of the winter mixed layer that is capped by warmer temperatures during summer. The seasonal thermocline capping the cold water is evident in the average sections (Fig. 4a, boxes 16 and 18). The coldest water over the shelf reaches a depth of approximately 200 m, overlaying warmer more saline water below. This is consistent with observations that the mixed layer can extend to 200 m during winter over the Labrador shelf (Fissel et al.

1989). The minimum temperature on the Labrador shelf is slightly lower, and the volume of cold water (e.g., $<0°C$) is significantly larger than on the west Greenland shelf. This difference might be attributed to the position of the boxes relative to sources of cold freshwater. For instance, box 16 is located downstream of Davis Strait and Hudson Strait (Fig. 2).

The transition from cold, fresh water over the shelf to relatively warm, salty water over the upper slope amounts to a horizontal temperature change of roughly 4°C and a salinity change of up to 1.5 at 100-m depth on the Greenland and Labrador shelves. The gradients on the Newfoundland shelf are approximately one-half as strong. These horizontal gradients result in the formation of a strong density front at the shelf break, as evidenced by the sharply tilted isopycnals in the upper 200 m of the water column. However, another interesting feature in the density fields for the northern boxes is the presence of the deep, steeply diving isopycnals adjacent to the upper slope (300–600 m, Fig. 4a). These isopycnals form a second, deep-reaching front located in the core of the Irminger Water.[3] The two fronts have very different origins: the shallow front is associated with the East/West Greenland Currents and Arctic water masses, while the deep front is associated with Irminger Water and is a downstream remnant of the Irminger Current. The Irminger front is steepest along the west Greenland slope (box 6), remaining steep along the Labrador slope (box 16), but begins to flatten out along the Newfoundland slope (box 18) where the erosion of the Irminger Water is almost complete.

b. Southern boxes

Downstream of Flemish Cap there are significant changes in the cross-shelf distribution of temperature and salinity (Fig. 4b). First, the deep isopycnals that are part of the Irminger front in the north flatten out completely (e.g., $\sigma_\theta = 27.65$ kg m^{-3}). At the Tail of the Grand Banks (box 21) there is a weak subsurface maximum in temperature near 550 m (see Fig. 6) but there is no significant cross-slope density gradient at depths below 350 m and no evidence of a subsurface salinity maximum to indicate significant presence of Irminger Water (Fig. 4b). West of the Grand Banks the warm, salty anomaly associated with the Irminger Water is absent (cf. Figs. 5a and 5b). In fact, the water on the upper slope at the Tail of the Grand Banks is much warmer and saltier than the Irminger Water in the same density class upstream of the Grand Banks (Fig. 5a), indicating that the progressive cooling and freshening associated with the eroding Irminger water mass has been interrupted at the Tail of the Grand Banks. This suggests that there is no advective tongue of Irminger Water that penetrates west of the Grand Banks.

The coldest shelf water at box 21 reaches values comparable to the coldest shelf water upstream ($\theta = -0.4°C$) but the cross-shelf distribution of temperature is markedly different than in the northern sections. For example, in box 21, the coldest and freshest water is trapped at the bottom over the shelf break and upper slope (Fig. 6). By comparison, the coldest water in box 18, on the Newfoundland shelf, is centered near 80-m depth, bounded by the seasonal thermocline near the surface and by warm Irminger Water at depth (Fig. 6). Between the Newfoundland shelf to the north and the Tail of the Grand Banks, the shelf break shoals from nearly 400 to 100 m, the shelf broadens and becomes uniformly shallow over the Grand Banks, and the continental slope steepens as the deep isobaths converge downstream of Flemish Cap (Fig. 2 and 6). As a result, the large volume of cold shelf water centered in the upper portion of the water column north of Flemish Cap becomes bottom trapped as the shelf topography shoals around the Grand Banks (e.g., cf. the 3°C isotherm in Fig. 6).

West of the Grand Banks, on the western Scotian shelf (box 24, Fig. 4b), the volume of cold water observed in the upper 400 m over the Labrador and Newfoundland shelves, associated with the Labrador Current, is almost completely gone. This is not surprising since, between boxes 21 and 22, a portion of the Labrador Current retroflects toward the east (Clarke et al. 1980). Downstream of this retroflection, the coldest water is limited to the upper 100 m, bounded above by the seasonal thermocline (box 24, Fig. 4b). This is consistent with the cold intermediate layer typically observed on the Scotian shelf between spring and autumn when winter-cooled water is capped by a warm surface layer resulting from seasonal heating (Loder et al. 2003). The outflow of relatively cold, fresh water from the Gulf of St. Lawrence, immediately upstream of box 24, is most likely responsible for the significant freshening that occurs over the shelf between the Tail of the Grand Banks and the Scotian shelf (Drinkwater et al. 2002).

Despite the fact that the Irminger Water is not discernable west of the Grand Banks, a subsurface temperature maximum appears over the western Scotian slope (box 24, Fig. 4b). This signal is much shallower (200 m) and warmer ($>8°C$) than the Irminger Water observed in the northern sections. Gatien (1976) iden-

[3] The deep front is also identifiable in high-resolution, synoptic CTD sections occupied by the authors on the west Greenland coast (within our box 6); hence it is not an artifact of the averaging process.

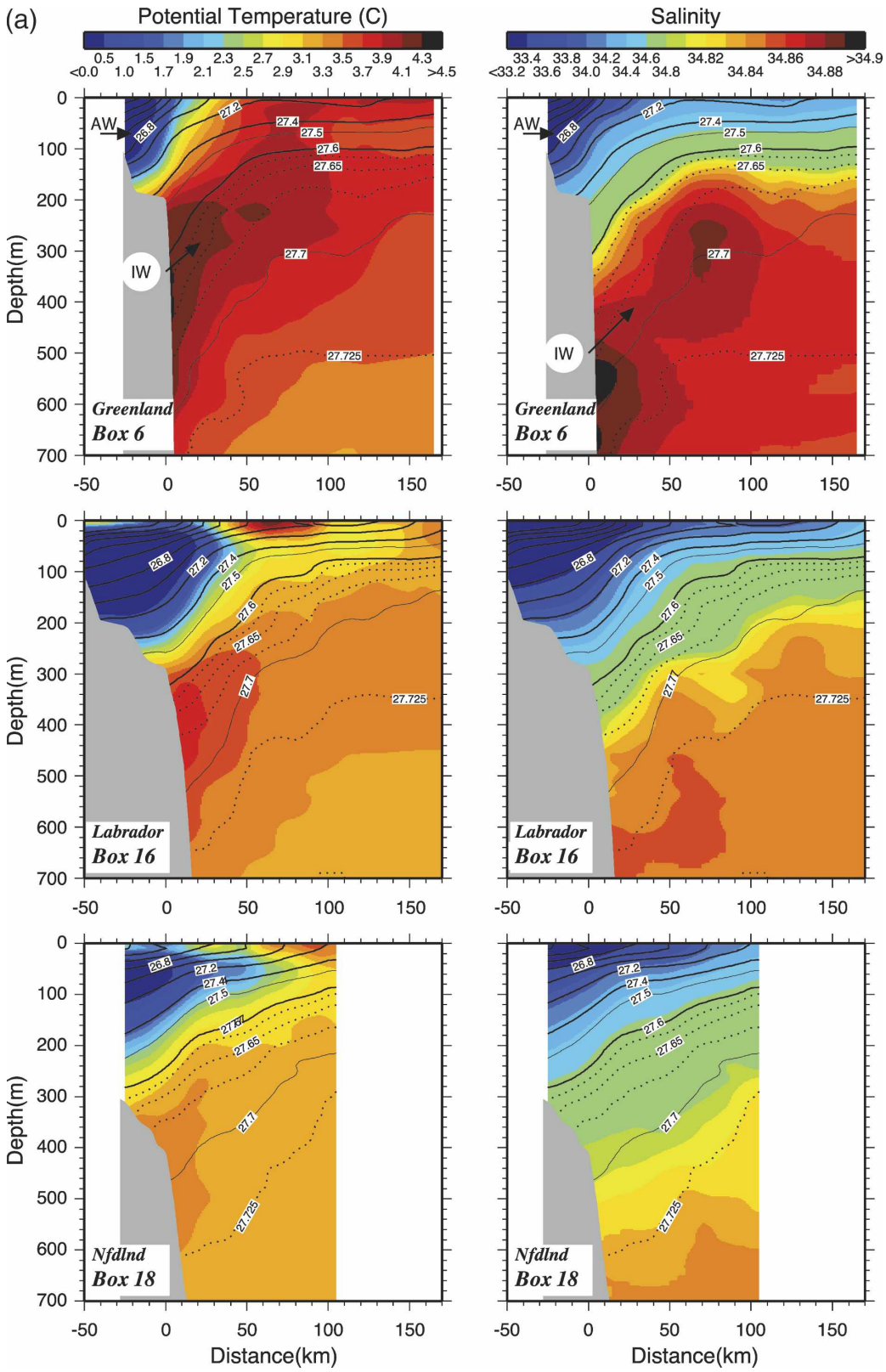

FIG. 4. Mean sections of (left) potential temperature (color), (right) salinity (color), and potential density (contours) for the (a) northern region and (b) southern region. See Fig. 2 for locations.

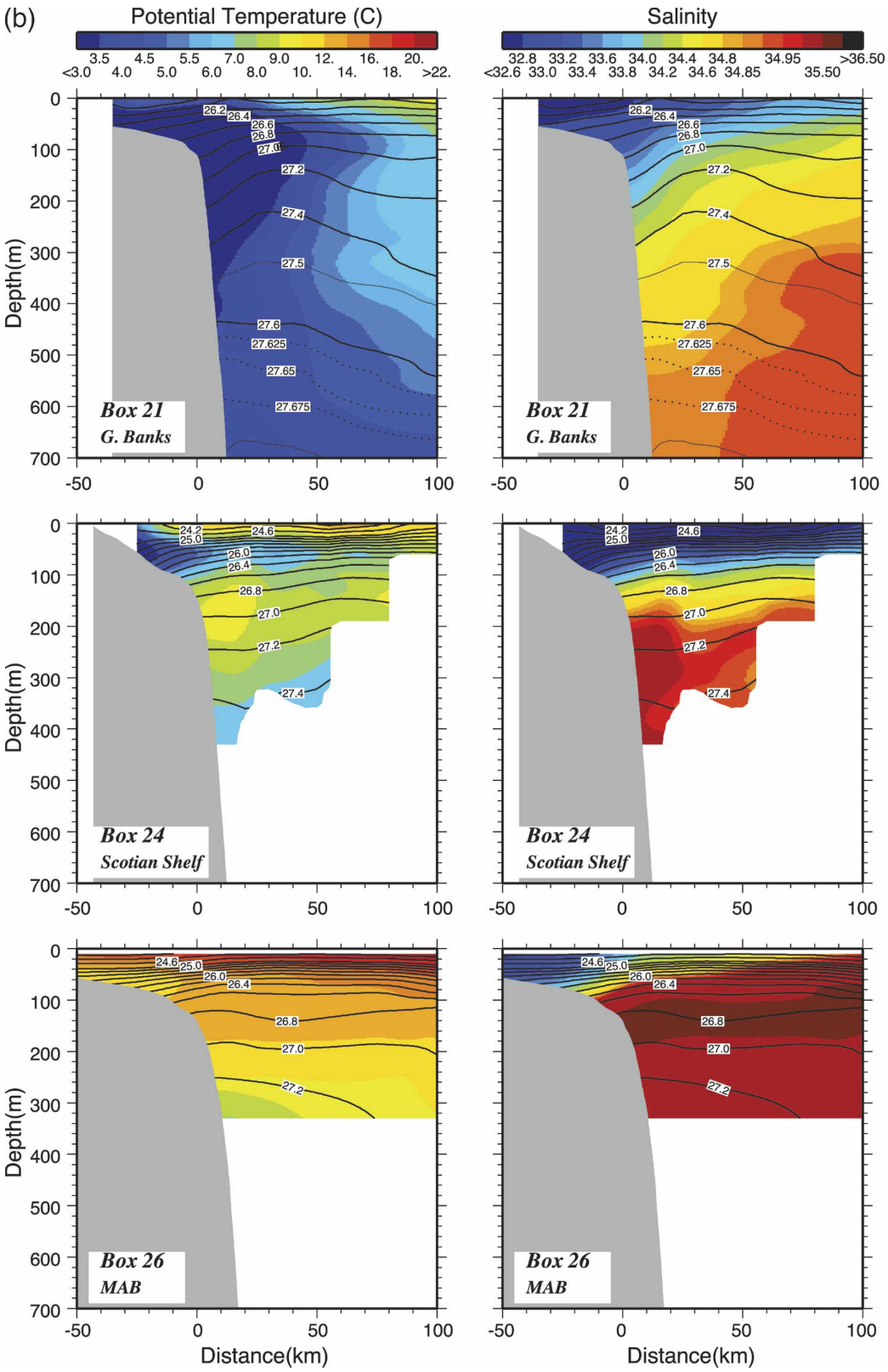

FIG. 4. (*Continued*)

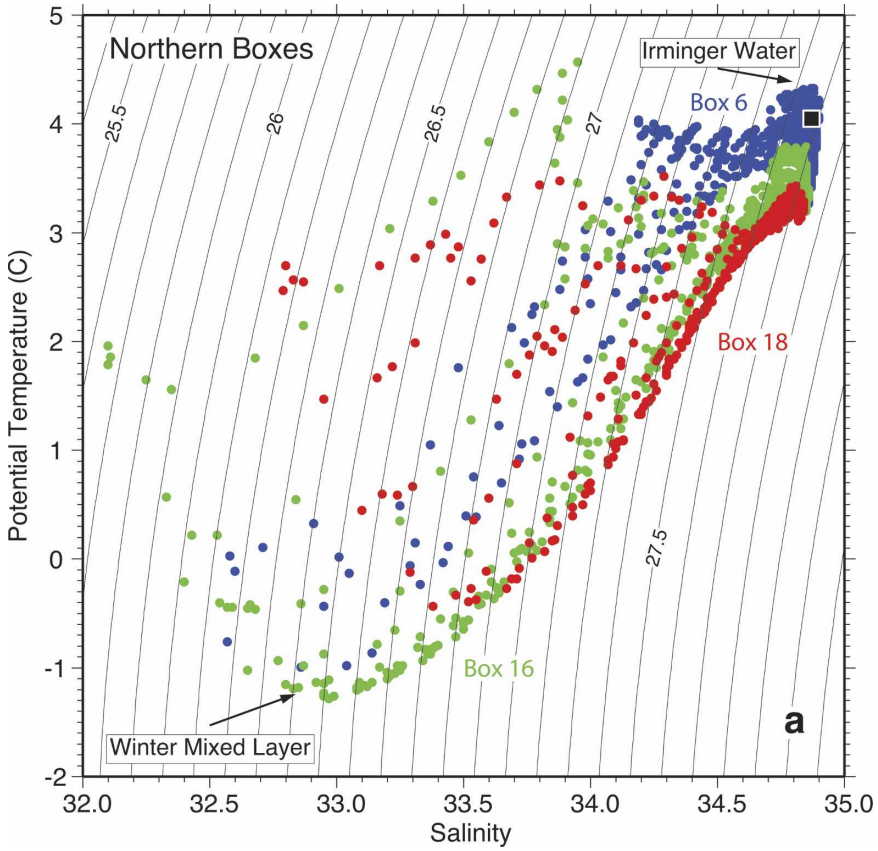

FIG. 5. The θ–S diagrams for the (a) northern and (b) southern sections in Fig. 4. The square in (a) denotes the average θ–S of water in box 21 [shown in (b)] having $\sigma_\theta > 27.60$ kg m^{-3}.

tified two types of water that reside inshore of the Gulf Stream on the continental slope between the Tail of the Grand Banks and Cape Hatteras: Labrador Slope Water, with temperatures typically 4°–8°C and salinities 34.3–35 psu, and "Warm Slope Water," with temperatures between 8° and 12°C and salinities 34.7–35.5 psu (Fig. 5b). Labrador Slope Water is primarily derived from Labrador Current water (100–300-m depth) entering the region from the east, while Warm Slope Water is a modified form of North Atlantic Central Water entering from the west (Gatien 1976). Aside from an event in 1998 when a large amount of cold Labrador Slope Water penetrated equatorward, warm slope water was observed along the Scotian shelf throughout the 1990s (Drinkwater et al. 2002). This is consistent with our results. Close to the Labrador Current retroflection, the slope water has properties consistent with Labrador Slope Water (box 21, Fig. 5b). While some trace of Labrador Slope Water is detectable at depth along the Scotian slope, overall the slope water in the upper 300–400 m becomes progressively warmer and saltier downstream of the retroflection region, approaching the characteristics of warm slope water along the western Scotian shelf (box 24, Fig. 5b).

By the MAB (box 26, Fig. 4b), the largest of the horizontal density gradients are concentrated in the upper 100 m and the vertical stratification is twice as large as the upstream sections, a result of the formation of the seasonal thermocline through summertime heating. Below the seasonal thermocline, there is a hint of a "cold pool" of relatively homogenous water over the shelf. This well-known feature is a remnant of the winter-cooled water on the shelf ($\theta < 12$°C) that is characteristic in this region during summer (Beardsley and Flagg 1976; Linder and Gawarkiewicz 1998). Aside from this feature, most of the thermal structure is associated with the seasonal thermocline that is established in the upper 50 m of the water column. As a result, the density structure in this region is largely determined by salinity. A sharp salinity front is centered at the shelf break, with a change of roughly 1.3 over a horizontal distance of 30 km (Fig. 4b). The 34.5 psu isohaline, typically chosen to represent the frontal boundary in this region (Linder and Gawarkiewicz

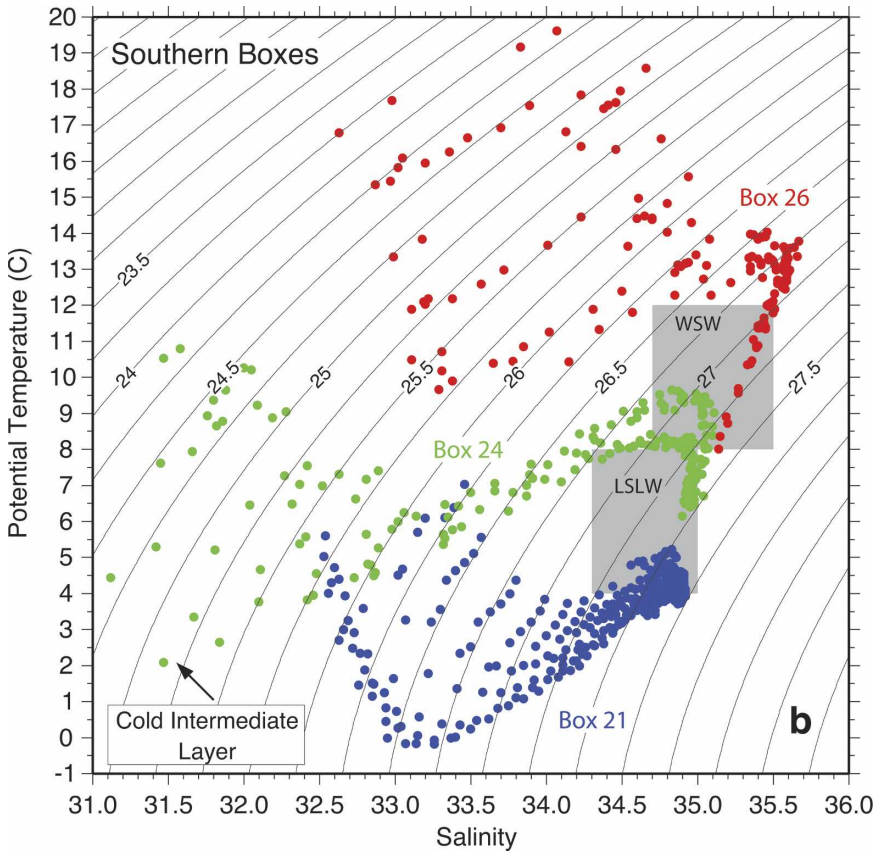

FIG. 5. (*Continued*) In (b), the θ–S ranges corresponding to Labrador Slope water (LSLW) and warm slope water (WSW) are denoted by the gray boxes.

1998), is located near the offshore edge of the front in Fig. 4b. Overall, the average MAB hydrographic section in Fig. 4b exhibits the canonical shelfbreak frontal pattern seen throughout this region (e.g., Linder and Gawarkiewicz 1998).

4. Velocity and transport evolution

While tracer measurements indicate that the northwestern Atlantic shelfbreak jet is a continuous current system (Chapman and Beardsley 1989), its velocity structure and transport vary significantly along its path from north to south (Loder et al. 1998). It is reasonable to expect such variability in light of the significant changes in cross-shelf density distribution observed in this climatology. Here, we make use of the good alongshelf resolution of our climatology to examine changes in the baroclinic velocity structure and transport of the shelfbreak current. Our goal is to determine whether the transport losses, highlighted by other studies [most notably Loder et al. (1998)], occur predominantly in a few select locations, or whether the current is leaky along its entire length.

Thermal wind fields were calculated in each regional box from the average hydrographic sections. Unfortunately, direct current observations were not available from the climate database to reference the thermal wind fields. Instead, we specified a reference depth for each thermal wind section that encompasses the majority of the baroclinic structure in the section, while remaining within the limits of the vertical data coverage. A reference level chosen deep enough to satisfy these constraints will intersect the steep topography on the continental slope. We follow the method introduced by Helland-Hansen (1934) to extend the thermal wind calculations into shallow water using a deeper reference level seaward of the shelf break [see also Mountain (1974)].

In the northern boxes the velocity was set to zero at 800 m, significantly deeper than the core of Irminger Water (typically centered near 400 m, Fig. 4a). In two of the northern boxes (boxes 15 and 19), the observations did not extend this deep (Table 1). In these cases, the maximum observation depth in the mean section was used instead (500 m). We acknowledge that this is not an ideal constraint since current velocities on the order

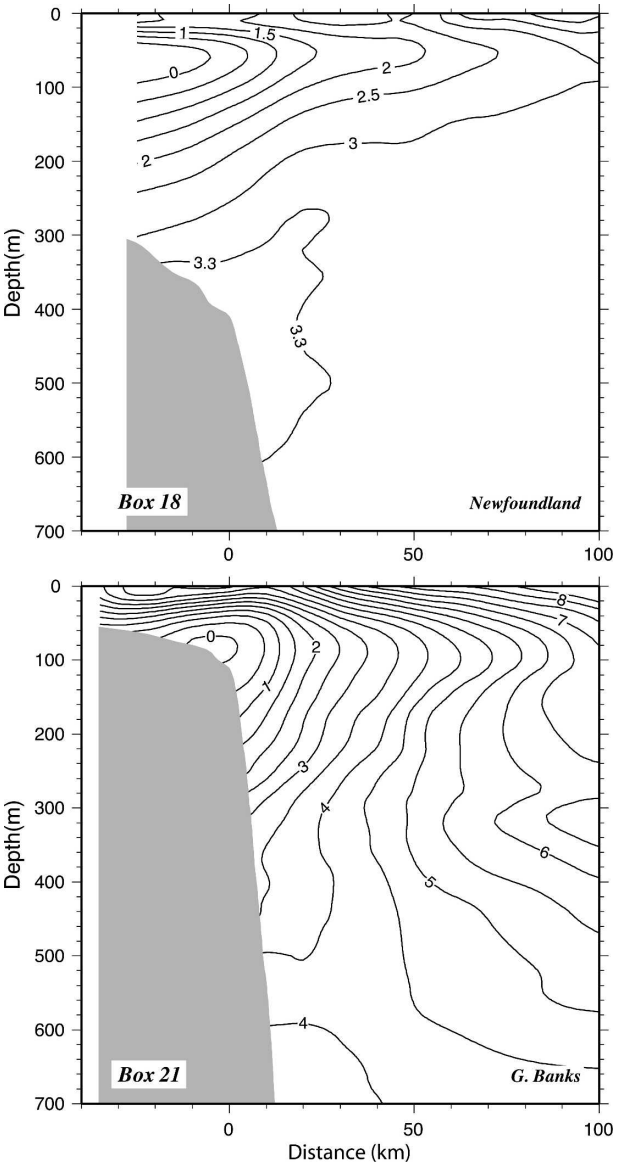

FIG. 6. Average potential temperature distribution in box 18, on the Newfoundland shelf, and in box 21, south of Flemish Cap.

of 10 cm s^{-1} have been observed at 700 m depth in both the West Greenland and Labrador Currents (Lavender et al. 2000; Cuny et al. 2002). As a result, the volume transport and magnitude of the jet are probably underestimated in the following calculations. Nonetheless, the resulting velocity fields should still allow us to quantify trends in baroclinic volume transport. For the southern boxes, the velocity was set to zero at the maximum observation depth, ranging from 200 m in the MAB to 800 m on the Scotian shelf. Without exception, the reference depths in the southern boxes encompassed all of the baroclinic structure associated with the shelfbreak front.

a. Velocity

Figure 7 shows the along-stream evolution of the baroclinic velocity field between the west Greenland shelf and the MAB. Note that, in all of our sections, distance is measured relative to the shelfbreak, increasing offshore. Using this convention, velocities in the shelfbreak jet are always negative whether the current is directed northward (as in the West Greenland Current) or westward (as in the MAB). In all of the sections, a jet is centered near the shelf break, although the structure and magnitude of the current is quite different from north to south. Notice that, even when the deep front is present, the thermal wind field resolves just one velocity core (Fig. 7a), suggesting that, regardless of water-mass origin, the original fronts have merged dynamically. In these cases, the baroclinic jet is rather broad, encompassing the combined width of both property fronts, and tilted seaward at depth. For example, along the west Greenland shelf the jet exceeds 30 cm s^{-1} near the surface and there is significant velocity shear to 500 m. Along the Labrador shelf, the core of the jet is shifted slightly offshore and the jet is broader at depth, with significant shear to 400 m. By contrast, the jet does not penetrate as deep in the south (Fig. 7b). At the Tail of the Grand Banks, the shelfbreak jet is narrower and only penetrates to 300 m. Here the equatorward flowing current is bounded on its seaward side by a broad region of poleward flow. This is probably the inshore edge of the slopewater jet; a branch of the Gulf Stream that bifurcates near 60°W (Csanady and Hamilton 1988; Pickart et al. 1999). Farther downstream, in the MAB, the shelfbreak jet is much weaker, with maximum velocity reaching just 12 cm s^{-1}, and the current is confined to the upper 100 m.

These differences are not surprising in light of the significant changes in the cross-slope density distribution that occur from north to south. In general, the jet is deeper and stronger in the sections containing the deep Irminger front. South of the Grand Banks, coincident with the disappearance of the deeper front and the erosion of the Irminger Sea Water, the jet weakens and becomes more confined to the upper water column. This raises the question: If the Irminger front is a downstream remnant of the Irminger Current, what portion of the transport loss in the shelfbreak system may be attributed to the weakening and disappearance of this front and its velocity contribution?

b. Transport

Using the average thermal wind fields constructed for each of the regional boxes, we calculated the transport of the baroclinic component of the shelfbreak jet

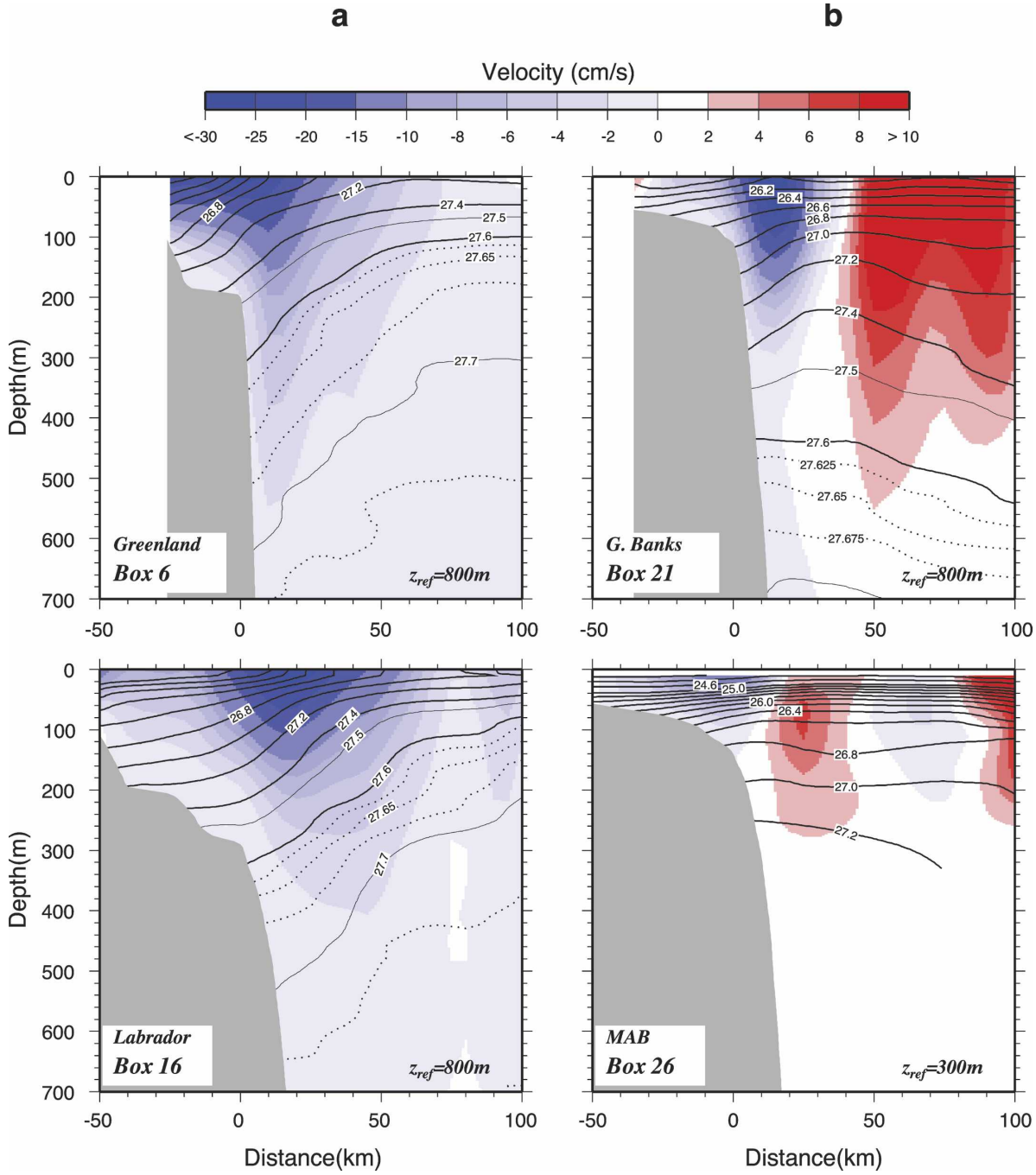

FIG. 7. (a) Thermal wind fields (color) calculated from the mean hydrographic sections for the west Greenland and Labrador shelves in the northern region. Contours of potential density are overlaid. Velocity is set to zero at z_{ref}. (b) As in (a) but for the Tail of the Grand Banks and the Middle Atlantic Bight in the southern region.

and documented its evolution over the path of the current (Fig. 8). The cross-stream limits on the transport calculation in each regional box were set where the equatorward velocity reaches a minimum value. We recognize that by using the referenced geostrophic velocity rather than absolute velocity we neglect a significant component of the transport in the shelfbreak current, particularly in the north. For instance, the barotropic component of the transport on the outer Labrador shelf can amount to as much as 65% of the total transport (Lazier and Wright 1993). Nonetheless, we can learn something about the nature of the trans-

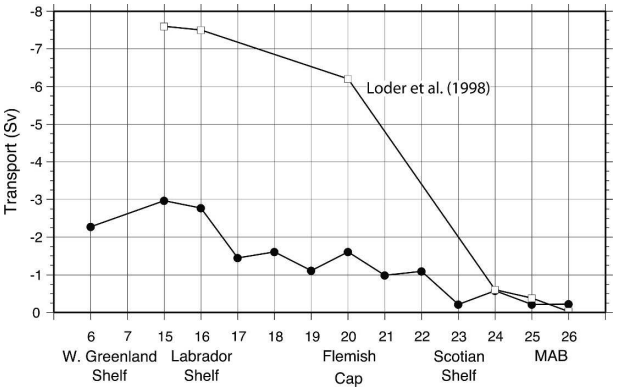

FIG. 8. Along-stream evolution of the baroclinic transport estimated from the average thermal wind field in each regional box (circles) with along-stream evolution of the total volume transport estimated by Loder et al. (1998; squares).

port loss in the shelfbreak system by examining alongshelf trends in the baroclinic transport.

In general, our baroclinic transport estimates are smaller than those reported in the literature (e.g., Lazier and Wright 1993; Colbourne et al. 1997; Petrie and Anderson 1983; Mclellan 1957; Smith et al. 1937; Petrie and Buckley 1996; Loder et al. 2003). However, most of these calculations use deeper reference levels than ours and include the transport over the entire shelf, not just at the shelf break. As noted earlier, current velocities on the order of 10 cm s^{-1} have been observed at depths comparable to our level of no motion. In addition, on the Labrador and Newfoundland shelves, an inshore branch of the Labrador Current may contribute up to 15%–20% of the total transport across the section and an even larger fraction of the total baroclinic transport in the section (Lazier and Wright 1993; Colbourne et al. 1997). This easily accounts for the differences between some of the historical estimates and ours, which are approximately 20%–30% lower. The differences between our estimates and those reported in previous studies become smaller equatorward of the Grand Banks. This is not surprising because, downstream of the Grand Banks, most of the deep baroclinic structure associated with the Irminger front has disappeared.

Overall, we find a decrease in baroclinic transport from north to south that is consistent with the alongshelf trend suggested by the regional studies (Fig. 8). Furthermore, the trend in baroclinic transport is consistent with the total transport loss characterized by Loder et al. (1998). In Fig. 8, the baroclinic transport decreases from roughly 3 Sv (Sv $\equiv 10^6$ m^3 s^{-1}) along the west Greenland and Labrador shelves to 0.25 Sv in the MAB. This amounts to a 90% drop in transport from north to south, comparable to the total transport losses reported by Loder et al. (1998). However, the details of the baroclinic transport loss are different. Loder et al. (1998) show that a majority of the total transport is lost around the Tail of the Grand Banks (~73% of the total), while a smaller amount is lost between the Labrador shelf and the Newfoundland shelf (~17%). In our climatology the baroclinic transport drops by roughly equal amounts on the southern Labrador shelf (boxes 16 to 17) and around the Tail of the Grand Banks (box 20 to 23). The latter transport loss can be attributed to the partial retroflection of the Labrador Current downstream of Flemish Cap (Clarke et al. 1980; Loder et al. 1998), with the largest decrease occurring between the Grand Banks and Scotian shelf (box 22 to 23). However, it should be noted that, if our transport estimate for box 23 were artificially low (e.g., due to topographic variability in this box), then the transport loss would appear to decrease more gradually between the Grand Banks and the MAB. While Loder et al. (1998) were unable to provide details on the transport loss between Hamilton Bank, on the Labrador shelf, and Flemish Cap, our results suggest that the shelfbreak jet loses baroclinic transport near 53°N. This is consistent with observations of surface drifter trajectories, which show a preference for detrainment in this region. Cuny et al. (2002) describe the trajectories of four drifters that left the Labrador Current between 52° and 55°N, first traveling north seaward of the shelf break and finally turning east to cross the Labrador Sea. Similarly, Reverdin et al. (2003) observed a preference for detrainment of surface drifters near 53°N. Drifter statistics compiled by Petrie and Anderson (1983) also support this, showing that drifters released near the shelf edge in this region uniformly left the shelf break, although they do not have trajectories to show where the drifters turned offshore. Similarly, the diagnostic model of Reynaud et al. (1995) shows fresh Labrador shelf water being transported offshore into the central Labrador Sea just north of here, near 55°N. Perhaps this detrainment is related to the topographic spur associated with Hamilton Bank where the isobaths undergo an eastward excursion (Fig. 2).

There is evidence in historical observations that, while detrainment likely occurs on the seaward side of the Labrador Current, transport may also be lost on the shoreward side of the current. Circulation patterns from dynamic topography and drifter trajectories suggest that a portion of the southward flow found between Hamilton Bank and the shelf break is consistently diverted shoreward around the southern end of Hamilton Bank (Colbourne et al. 1997; Lazier and Wright 1993). Colbourne et al. (1997) found that a large number of surface drifters launched inshore of the 600-m isobath east of Hamilton Bank (our box 16) were

consistently diverted onshore to join the weaker inshore branch of the Labrador Current. Most of these drifters eventually rejoined the main branch of the Labrador Current at the shelf break immediately north of Flemish Cap (roughly box 19 in our climatology), although a few continue to follow an inshore pathway around the southern tip of Newfoundland. A similar circulation pattern is observed in diagnostic models of the northwestern Atlantic (e.g., Reynaud et al. 1995). The transport loss in our climatology takes place between the southern end of the Labrador shelf (box 16) and the northern end of the Newfoundland shelf (box 17). According to drifter trajectories, it is between these two regional boxes that the inshore branching of the current occurs. Our method of collapsing sections onto a standard grid does not allow us to resolve the details of the flow field along the inner shelf. Hence we are unable to account for the transport that might be lost to the inshore branch of the Labrador Current. However, if this splitting were the cause of the observed transport drop in Fig. 8 between the Labrador and Newfoundland shelves, we would expect to see the transport increase again along the Newfoundland shelf where a majority of the inshore branch rejoins the Labrador Current at the shelf break (Colbourne et al. 1997). Instead, the baroclinic transport remains roughly constant after the initial drop, eventually decreasing again south of Flemish Cap. Hence, we expect that this is not the cause of the transport loss observed in our climatology. The Strait of Belle Isle, the channel between the Labrador coast and Newfoundland, does support a small net inflow from the inner shelf into the Gulf of St. Lawrence (Petrie et al. 1988). However, observations indicate that the transport through the Strait of Belle Isle is too small to account for the transport loss that is observed at the shelf break in this location. Therefore, we suspect that the transport loss is the result of offshore, rather than onshore, detrainment.

The relative contribution of baroclinic and barotropic transports to the total volume transport of the shelfbreak jet varies from north to south. Therefore, the trends in Fig. 8 are not necessarily representative of the along-stream trends in total volume transport. In a low-passed sense, the changes in baroclinic transport may be represented by two large drops separated by plateaus in the north (boxes 16–17), in the middle of the domain (boxes 17–20), and in the south (boxes 23–26). Comparing this with the only existing domainwide total transport estimates (Loder et al. 1998; Fig. 8), we find that the baroclinic transport amounts to 34% of the total transport along the Labrador shelf, 22% of the total along the Newfoundland shelf, and 55% of the total along the Scotian shelf and MAB. These ratios are consistent with the breakdowns from independent observations. For instance, Lazier and Wright (1993) estimate that the baroclinic component of the transport in the Labrador Current (not including the inshore branch) amounts to roughly 35% of the total transport at the shelf break. By comparison, the transport calculations by Colbourne et al. (1997) along the Newfoundland shelf break and Greenberg and Petrie (1988) in Flemish Pass suggest that the baroclinic transport in the shelfbreak current (again, not including the inshore branch) make up roughly 20% of the total. Farther downstream, recent studies have shown that the majority of equatorward flow along the Scotian shelf and in the MAB can be diagnosed from density fields alone (Han et al. 1997; Hannah et al. 1996; Fratantoni et al. 2001). Fratantoni et al. (2001) calculated the total transport of the shelfbreak jet in the MAB south of Nantucket using a collection of absolute velocity sections measured by a shipboard acoustic Doppler current profiler (ADCP). We used these observations to determine the relative contributions of the baroclinic and barotropic components to the total transport in the MAB, concluding that the baroclinic transport amounts to 53% of the total transport at this location, consistent with our estimate above.

Our results, as well as regional studies, indicate that the relative importance of the baroclinic transport decreases between the Labrador shelf and the Grand Banks and increases along the Scotian shelf, reaching a maximum in the MAB. Scaling our baroclinic transports as such has the effect of increasing the magnitude of the transport loss around the Tail of the Grand Banks relative to the transport loss in the northern portion of the domain, resulting in the same trends that were described by Loder et al. (1998). However, the higher resolution of the climatology enables us to refine the historical estimates. The overall picture from our climatology is that baroclinic transport is predominantly lost from the shelfbreak current in two locations: between the southern Labrador and northern Newfoundland shelves, and around the Tail of the Grand Banks.

5. Frontal evolution

We have shown that the western North Atlantic shelfbreak front consists of a shallow front that is present throughout the domain (the main shelfbreak front), but also includes a deeper component (the Irminger front) in the north. The structure of the baroclinic velocity field, consisting of a single velocity core, suggests that the dynamics of the two property fronts have most likely become intertwined on the southern Labrador and Newfoundland shelves. Nevertheless,

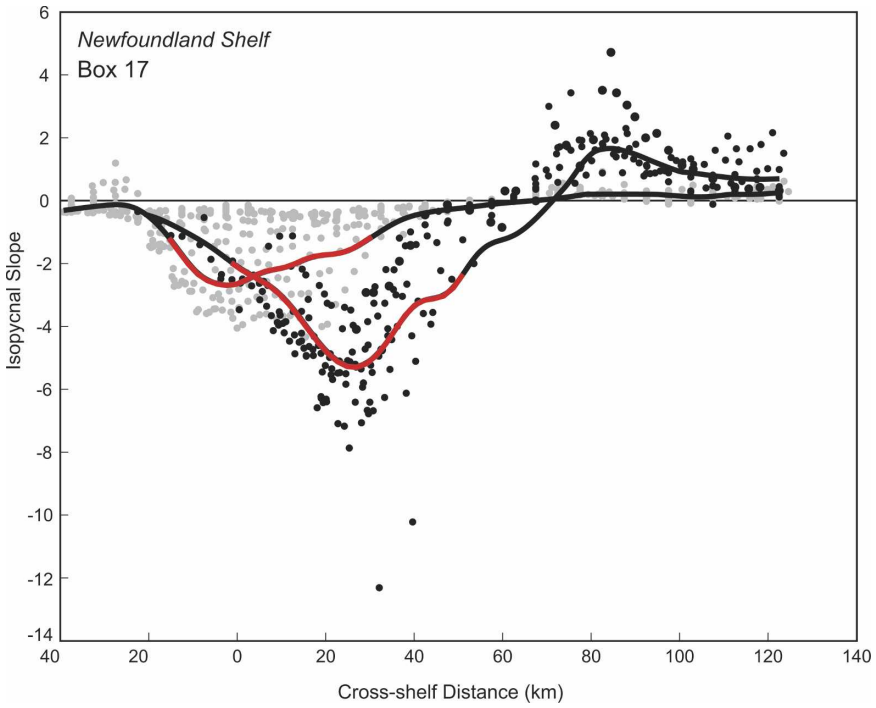

FIG. 9. The isopycnal slope vs offshore distance at each grid point in the average density section for box 17 on the Newfoundland shelf. The two clusters of steep slopes associated with the inshore ($\sigma_\theta < 27.5$ kg m^{-3}) and Irminger ($\sigma_\theta > 27.5$ kg m^{-3}) fronts are denoted by the gray and black points, respectively. The heavy black lines are low-passed curves fit to the two peaks in the data. The *e*-folding width of the low-passed curves is shown in red.

the main shelfbreak front and deeper Irminger front are distinguishable in temperature and salinity in the northern domain. Hence, it is interesting to compare the characteristics of the two fronts as they evolve from north to south. To do this, we have developed an objective method for identifying the position of the density front in each average section. Our method allows for the separate identification of the two fronts discussed above. Knowing the position of these fronts, we are then able to identify the characteristics of the front at each location (e.g., central isopycnal, temperature, salinity, and grounding position). In this section we outline the method used to determine the position of the front, and then discuss the variation in frontal characteristics from region to region.

To identify the position of the front in a given section, we assume that the front is located where the isopycnals are most steeply sloped. To find this location, we compute the slope of each isopycnal, progressing across the mean density section for each box, and construct a scatterplot of the values versus cross-shelf distance. The distribution of points will reveal a peak near the center of the front with smaller isopycnal slopes inshore and offshore of this position. As an example, we show the isopycnal slopes calculated for box 17 on the northern Newfoundland shelf (Fig. 9). The slope calculation results in two clusters of steep slopes separated by the $\sigma_\theta = 27.5$ kg m^{-3} isopycnal: the first near the shelfbreak at $x = 0$ km, and the other farther offshore near $x = 25$ km. These two groups are easily separable and correspond to the shallow shelfbreak front and deeper Irminger front previously discussed. To quantify the cross-shelf position corresponding to the greatest isopycnal slope, we used a low-passed curve for each set of points. In sections where the two fronts are identifiable in the scatterplots, two separate low-pass curves are computed as shown in Fig. 9. In each of these cases the dividing isopycnal was $\sigma_\theta = 27.5$ kg m^{-3}, separating the shelfbreak and Irminger regions.

Once the cross-shelf position of the front has been identified, we examine the isopycnals in the vicinity of this location to pinpoint the central isopycnal and its depth. Specifically, the slopes of all isopycnals falling within δx of the central x position (where δx is the *e*-folding width of the low-passed curve, above) are plotted, and the ensemble of isopycnals with the largest slopes is identified. The central isopycnal is calculated as the average of this group. The results for our example, using the mean section from box 17, are plotted in Fig. 10 where the two circles correspond to the cen-

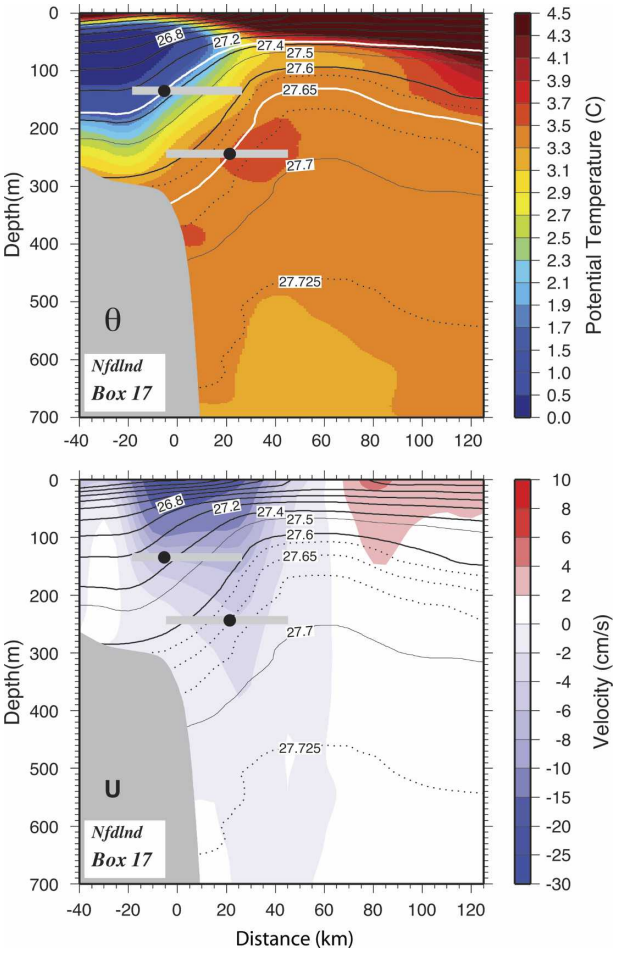

FIG. 10. (top) Mean potential temperature distribution with contours of potential density for box 17 on the Newfoundland shelf. (bottom) Thermal wind field calculated for box 17 (colors), assuming zero velocity at 800 m with contours of potential density. The location of the two density fronts are denoted by black circles, and the width of the fronts are specified by the gray bars. The central isopycnal in each front is contoured in white.

tral position of the main shelfbreak and Irminger fronts. The solid gray lines correspond to δx, representing the width of each front. The central isopycnal for each front is contoured in white. Note that the slope of the Irminger front is steeper than the main front, consistent with the two peaks in Fig. 9. We found this to be true for all cases when the Irminger front was present. Even though the central positions of the two fronts are offset by more than 100 m in depth, their widths overlap. Hence, it is not surprising that the thermal wind field, referenced to zero at 800 m, shows just one velocity core (Fig. 10).

While the isopycnal slopes in the Irminger front were consistently steeper than those in the main shelfbreak front, the density changes across the Irminger front were considerably less (roughly 0.2 kg m^{-3} as compared with 1.0 kg m^{-3}). An alternate method to define the position of the front would be to search for the maximum cross-shelf density gradient (σ_x) in each average section. However, this method is complicated by the presence of the seasonal pycnocline during summer. We found that the largest density gradients in the average sections were often located near the surface, in the seasonal pycnocline, rather than in the shelfbreak front. Hence, identifying the position of the front based on isopycnal slopes proved to be a more reliable method for objectively locating the subsurface front in each section.

a. Frontal temperature and salinity

Using the central positions identified from each mean section, we are able to track the along-stream variation in temperature, salinity, and density within both fronts. Figure 11a illustrates the evolution of the θ–S relationship. As illustrated by the example in Fig. 9, the $\sigma_\theta = 27.5$ kg m^{-3} isopycnal divides the main shelfbreak regime from that of the Irminger front. The main front is always less dense than 27.5 kg m^{-3}. Note that the along-shelf changes in temperature and salinity are an order of magnitude larger in the main front ($\Delta\theta \sim 12$°C and $\Delta S \sim 1.5$) when compared with the Irminger front ($\Delta\theta \sim 1$°C and $\Delta S \sim 0.2$). To determine the significance of these along-stream property variations, we examined the temporal (interannual and/or seasonal) variability at a single location. In particular, the position of the two fronts and their properties were identified for a collection of synoptic sections within a single box. This indicates that the density of the Irminger front may vary by up to 0.1 kg m^{-3}, with temperature and salinity varying by up to 1.4°C and 0.2.

The character of the observed property variation is markedly different for the two fronts. The θ–S variation of the Irminger front shows that it cools and freshens between the west Greenland coast and Flemish Pass (Fig. 11a, inset). Even though the interannual variability in the Irminger front can be as large as these along-stream changes, the changes are consistent with the gradual erosion of the Irminger water mass described earlier. As the Irminger front cools and freshens, the changes in temperature and salinity are compensating and the density remains roughly constant (Figs. 11a,b). This suggests that the Irminger Water is eroded through isopycnal mixing. The only exception is box 7. However, observations suggest that this is the location where the West Greenland Current is diverted from the coast across the basin toward the Labrador shelf (Cuny et al. 2002; Reverdin et al. 2003). Indeed, the majority of the climatological sections located in box 7 (Fig. 3) are aligned parallel to the deep isobaths, suggesting

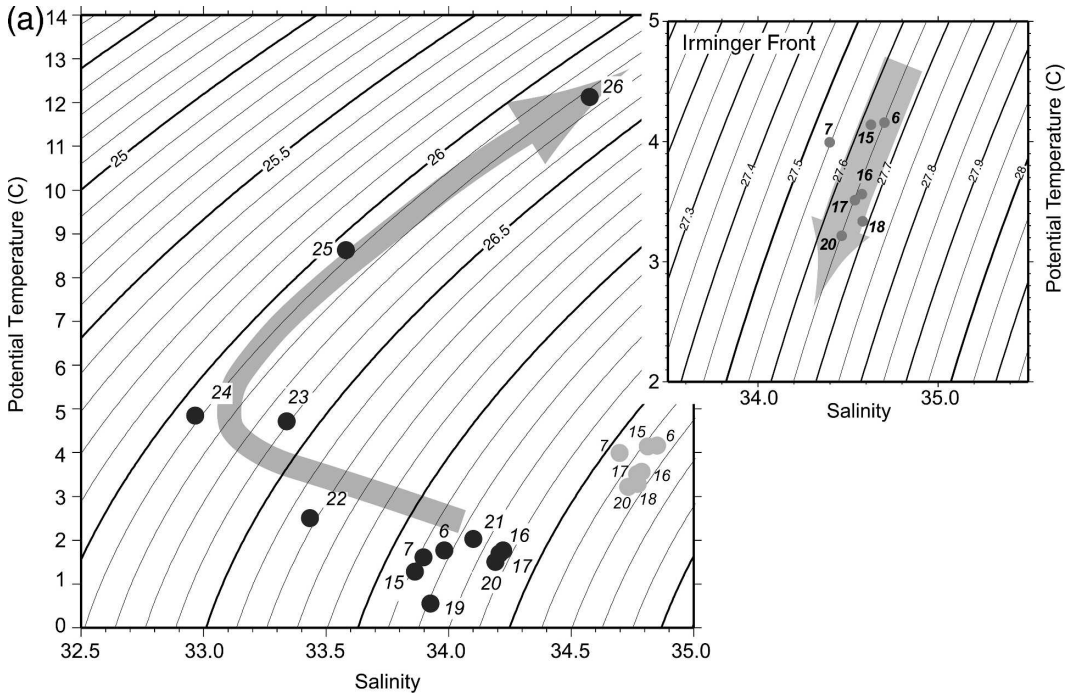

FIG. 11. (a) The θ–S diagram of the properties within the inshore (black circles) and Irminger (gray circles) fronts. Each point represents the properties at the center of the front from the average section in each regional box as determined by isopycnal slope analysis (the numbers next to each point correspond to the box number.) The θ–S properties in the Irminger front are shown in greater detail in the inset. The general progression of the alongshore property changes in both fronts are indicated by the arrow.

that the average density section is aligned somewhat tangential to the front rather than crossing it. As a result, the isopycnal slopes in box 7 are significantly reduced compared with box 6, immediately upstream (not shown).

In comparison with the Irminger front, the main shelfbreak front exhibits both larger along-stream and interannual variability. For instance, the density of the front may vary by up to 0.45 kg m^{-3} interannually, with changes in temperature and salinity of 3.5°C and 0.6. This suggests that only the changes equatorward of the Grand Banks are significant (Fig. 11a). Between the Grand Banks and western Scotian shelf the front warms, freshens, and becomes less dense (Fig. 11b). While it is tempting to attribute the freshening to the Gulf of St. Lawrence (Khatiwala et al. 1999), we note that this trend begins upstream of the channel, suggesting that the outflow from the Gulf of St. Lawrence is only part of the story. This is discussed further in section 6. The influence of outflow from the Gulf of St. Lawrence is clear in Fig. 4b, where a large plume of low salinity water extends out to 100 km offshore of the shelf break in box 24 with salinities up to 1.5 lower than the freshest shelf water in box 21 (Fig. 5b). By comparison, the freshest water in box 21 is confined to the shelf (e.g., cf. the 33.0 psu isohaline in Fig. 4b). This is consistent with climatological maps of surface salinity for the northwestern Atlantic that show the freshest water confined to the shelf along the Labrador and Newfoundland shelves, extending offshore between the Tail of the Grand Banks (our box 22) and the Gulf of Maine (our box 25), and finally returning to the shelf in the southern MAB (Loder et al. 1998).

Farther downstream, in the MAB, the main shelfbreak front varies in a different fashion. Here both temperature and salinity of the front increase equatorward, downstream of the Gulf of Maine (boxes 24–26, Fig. 11b). The rise in temperature and salinity between boxes 24 and 25 most likely results from vertical mixing that occurs in the Gulf of Maine between warm/salty Scotian slope water, entering the gulf through the Northeast Channel, and cold/fresh Scotian shelf water (Brown and Beardsley 1978). Farther downstream, the changes in frontal properties are most likely due to the close proximity of the Gulf Stream offshore. However, the changes in temperature and salinity throughout the MAB are generally compensating and the density in the front remains nearly constant (Fig. 11b). Hence, the overall picture of the along-stream density evolution of the front is similar to a step function with relatively

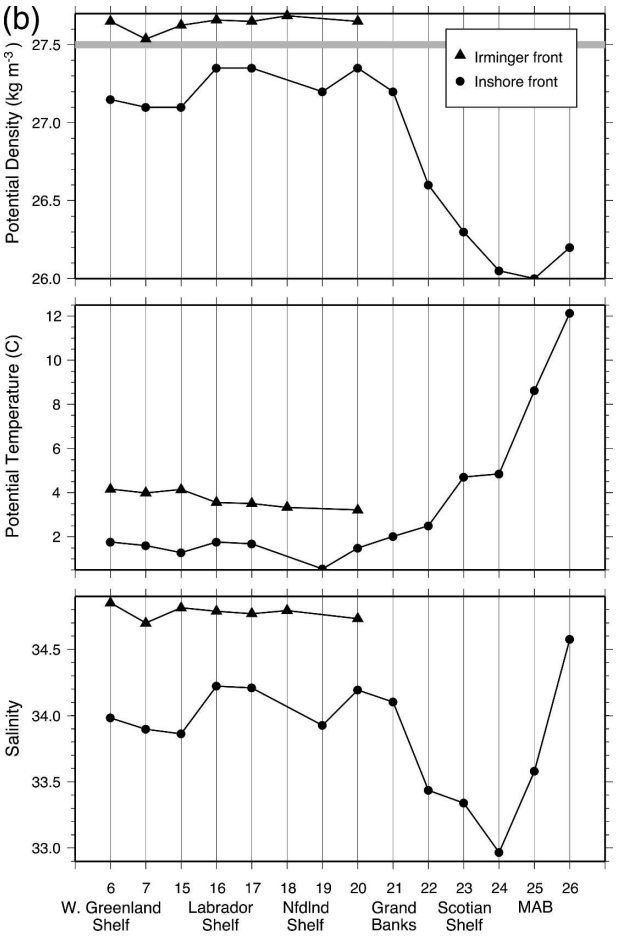

FIG. 11. (*Continued*) (b) Along-stream evolution of (top) potential density, (middle) potential temperature, and (bottom) salinity for the inshore (circles) and Irminger (triangles) front. The values are taken from the center of the front based on isopycnal slope analysis as described in the text. No point is plotted for regional boxes in which a front could not be identified. The thick gray line highlights the 27.5 kg m^{-3} isopycnal.

constant density poleward of the Grand Banks, a rapid decrease around the Tail of the Grand Banks, and nearly constant density in the MAB. It should be noted that the density typically associated with the shelfbreak front in the MAB is 26.5 kg m^{-3} (Linder and Gawarkiewicz 1998). Although the density of the front in boxes 25 and 26 is less than this (26.1 kg m^{-3}), the difference is within our estimate of interannual variability for the front. Figure 11b suggests that the Tail of the Grand Banks is a geographically critical point in the shelfbreak system, associated with large shifts in the properties of the main shelfbreak front. This will be further explored in the discussion in section 6.

b. Frontal grounding position

Based on the historical literature, one gets the impression that the front is more or less tied to the shelf break (hence its name). Progressing from north to south the shelf break shoals considerably, but there has been no study to date that investigates whether the front and jet follow this trend. Indeed, there are relatively few observations that track the grounding position of the shelfbreak front and none, that we are aware of, that catalog the position of the front along its full path. Wright (1976) used a 30-yr collection of salinity observations to document the monthly mean position of the shelfbreak front in the MAB. Using the 35-psu isohaline as a proxy for the position of the front, he found that the front intersected the bottom within 16 km of the shelf break 84% of the time. There is no indication in his results that the front preferentially grounded inshore or offshore of the shelf break. Linder and Gawarkiewicz (1998) also tracked the grounding position of the front, defined by the 34.5-psu isohaline, in a climatology of the MAB. They found that, regardless of season, the front intersects the bottom on or near the shelf break between Georges Bank and New Jersey. In bimonthly averages, the foot of the front was consistently located within 10 km of the shelf break. In contrast, the bulk of the jet appears to reside seaward of the shelf break in the Labrador Sea (Lazier and Wright 1993) and along the Scotian shelf (Loder et al. 2003).

Using the central isopycnal identified in each of the mean density sections, we now compare the grounding position of the two fronts with trends in topographic variability. Figure 12a shows the cross-shelf position where the two fronts ground in each regional box, as well as the local width of the shelf. The shelf break is located at 0 km, with distance increasing offshore. Positions are not shown in boxes where the central isopycnal did not intersect the bottom within the gridded region. Figure 12b compares the water depth where the grounding occurs with the water depth at the shelf break for each box. It is not surprising that the deeper Irminger front generally grounds offshore of the shelf break in the northern boxes. However, it is interesting that, except at the Grand Banks (where the depth of the shelf break decreases by 150 m), the main front consistently grounds within 20 km inshore of the shelf break. It follows that the depth of the grounding mirrors the along-stream trend in shelfbreak depth, first deepening and then shoaling from north to south (Fig. 12b). Overall then, the foot of the shelfbreak front remains trapped at the shelf break regardless of the width of the shelf, the depth of the shelf break, and the steepness of the slope. This implies that the continental shelf break does indeed play a dynamical role in determining the position of the front.

Modeling studies have suggested that the cross-isobath position of the shelfbreak front is determined

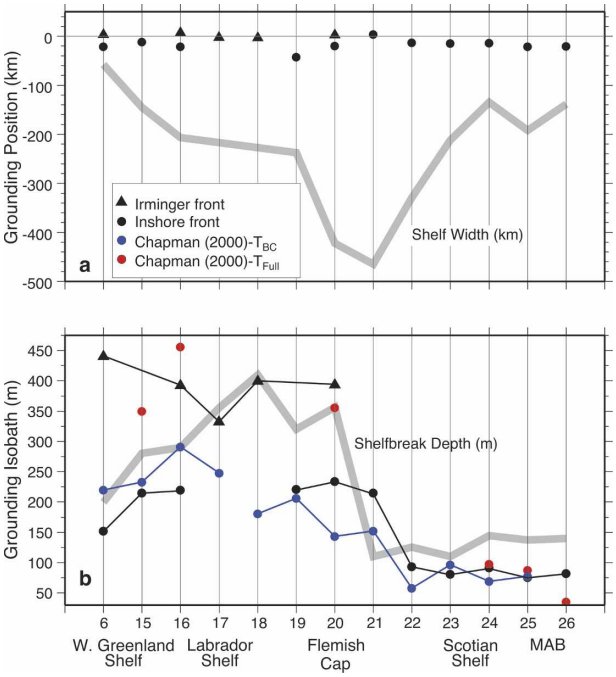

FIG. 12. (a) Grounding position (km) of the central isobath identified in the inshore (circles) and Irminger (triangles) fronts from the average section in each of the regional boxes. The grounding positions are measured relative to the shelf break with distance increasing offshore. The thick gray curve is the width of the shelf measured from the shelf break to the coast. No position is plotted in boxes where the central isopycnal did not ground within the bounds of the vertical section. (b) Water depth (m) at the positions in (a) (black) and predicted trapping depth of the shelfbreak front based on Chapman (2000) using baroclinic transport in blue and the total volume transport from Loder et al. (1998) in red. The thick gray curve is the depth of the shelf break estimated from high-resolution bathymetry data (see text).

by a trapping mechanism involving offshore buoyancy advection within the frictional bottom boundary layer. While Gawarkiewicz and Chapman (1992) argue that the presence of the shelf break is of fundamental importance to this process, a similar frontal trapping occurs in the model of Chapman and Lentz (1994) with a constant bottom slope. In the latter, a surface-to-bottom density front, formed by the input of buoyant water onto an unstratified shelf, is initially advected offshore by downslope Ekman transport in the frictional bottom boundary layer. As the front moves farther offshore, the geostrophic adjustment of the alongshelf current leads to a flow reversal near the bottom, resulting in a reversal in the Ekman transport and strong convergence in the bottom boundary layer. The front is ultimately trapped at this isobath. Chapman (2000) builds on these results by adding ambient offshore stratification and demonstrates that the trapping isobath (h_*) can be determined as a solution of

$$\frac{2N^2}{3g'}h_*^3 + h_*^2 - \frac{2T_o f}{g'} = 0,$$

where T_o is the baroclinic transport in the front, f is the Coriolis parameter, N is the buoyancy frequency of the ambient water seaward of the front, and $g' = g\Delta\rho/\rho_o$, with g being the gravitational acceleration, $\Delta\rho$ being the cross-frontal density gradient, and ρ_o being the average density in the front. One of the most interesting results from Chapman's (2000) study is that the trapping isobath and basic frontal trapping mechanism appear to be the same regardless of whether or not a shelf break is present. Is this at odds with our results?

Using the average sections from our climatology and baroclinic transport estimates from Fig. 8, we estimated the trapping depth predicted by Chapman's (2000) theory and compared this with the observed grounding depth in Fig. 12. Overall, the agreement between the predicted and observed grounding depth is quite good. Both exhibit similar large-scale trends, starting deep north of Flemish Cap and shoaling to lower values along the Scotian shelf and into the MAB. These trends roughly mirror the along-shelf trends in shelfbreak depth. Is this a coincidence? Chapman (2000) wonders if the cross-frontal density gradient, ambient stratification, and/or the transport of the jet continually adjust so that the trapping depth coincides with the shelf break. To answer this we evaluated the relative importance of each of these terms on the downstream evolution of h_*. We find that the evolution of the baroclinic transport is the dominant factor. As discussed above, there is a large baroclinic transport loss as the current rounds the Tail of the Grand Banks coincident with the shoaling of the shelf break. Hence, insofar as changes in the topography dictate transport variations of the current as our study suggests, this implies that, even in the framework of Chapman (2000), the shelf break will play a crucial role in determining the grounding position of the front.

It should be noted that we have used the baroclinic transport, instead of the total transport in the jet, to predict the trapping depth of the front [as did Chapman (2000)]. To examine the influence of the barotropic component on the proposed theory, we repeat the calculation using the total volume transport reported by Loder et al. (1998) (Fig. 8), together with the average sections in our climatology. While the overall trend remains the same (deeper grounding north of Flemish Cap and shoaling through the MAB), the theory overestimates the depth of the grounding isobath in the north where substantial barotropic flow exists (Fig. 12b). This suggests that the frontal trapping theory developed by Chapman (2000) cannot be applied as such

using the full transport. This is not surprising since adding a substantial barotropic component to the velocity field might well alter the convergence/divergence patterns in the bottom boundary layer that are inherent to the theory. Rasmussen et al. (2005) showed that Chapman's (2000) frontal trapping theory accurately predicted the grounding depth of the shelfbreak front using the full transport, but their observations came from the MAB where the baroclinic flow dominates and the theory does well even with the full transport (Fig. 12b).

6. Discussion

In this study we have presented a mean three-dimensional description of the summer shelfbreak front and jet, quantifying the along-stream evolution in structure, baroclinic transport, properties, and cross-stream position from the west coast of Greenland to the MAB. Our results demonstrate that there are actually two fronts in the northern part of the domain: the main front located near the shelf break, having origins in the East/West Greenland Currents and Arctic water masses, and a deeper front centered in the core of Irminger Water over the upper slope, originating as the Irminger Current east of Greenland. Despite their separate origins, the baroclinic velocity structure associated with the fronts consists of a single velocity core located near the shelf break. While the main shelfbreak front is present throughout the domain, the Irminger front gradually weakens as the Irminger water mass erodes, disappearing altogether near the Grand Banks. Despite its persistence, the structure of the main shelfbreak front and its properties exhibit large variations from north to south, with the largest changes occurring near the Tail of the Grand Banks. Interestingly, even with these large structural changes and despite significant topographic variability along its path, the bottom position of the main front remains trapped at the shelf break.

Our results indicate that the Tail of the Grand Banks is a geographically critical point in the shelfbreak system. It is the location where large topographic changes occur, including broadening of the shelf, shoaling of the shelf break, and steepening of the continental slope. These topographic changes force a significant portion of the main branch of the Labrador Current to leave the western boundary, taking with it a large amount of relatively cold, fresh water. The Grand Banks is also the southernmost location where any remnant of Irminger Water is observed. What happens to the recirculated Irminger Water? The Labrador Sea gyre is bounded to the south by the northwest corner of the North Atlantic Current, which penetrates to roughly 52°N offshore of the Labrador shelf (Fig. 1) (Lazier 1994; Kearns and Rossby 1998). Both surface drifter and subsurface float trajectories suggest that water originating in the shelfbreak jet leaves the boundary between 55°N and Flemish Cap to become trapped in offshore recirculating cells or eventually leaves the basin by joining the North Atlantic Current farther to the east (Fischer and Schott 2002; Cuny et al. 2002; Lavendar et al. 2000). This is consistent with our results, suggesting that what remains of the Irminger Water over the upper Labrador slope is recirculated with the northern extension of the North Atlantic Current north of Flemish Cap.

The Tail of the Grand Banks is also associated with a sharp change in the properties of the main shelfbreak front. Between the west Greenland shelf and the Newfoundland shelf, the center of the front is defined by roughly the same isopycnal. However, starting at the Tail of the Grand Banks, the front becomes fresher and less dense. We have confirmed that this signal is robust and that there is no temporal bias in our climatology introduced by interannual variability. On the Scotian shelf, the salinity gradients in the front are much sharper due to the contrast between the large input of freshwater by the Gulf of St. Lawrence on the shelf and the saltier slope water trapped offshore. One is tempted to conclude that the property shift in the front is simply due to the influence of this freshwater source. However, on closer inspection, the salinity in the front begins to decrease upstream of the Laurentian Channel, on the Tail of the Grand Banks. This prompts us to look for another explanation. As discussed earlier, the shoaling of the topography in the Grand Banks forces a significant portion of the Labrador Current water onto the upper slope where it subsequently retroflects. The water that is advected offshore by this process is the outer "salty" portion of the front (Fig. 4b, box 21). Hence, the shelfbreak front downstream of the Grand Banks is made up of the remaining fresher portion of the front.

Historical observations indicate that the Tail of the Grand Banks is the location of another transition in the shelfbreak system, namely, a shift in the cross-slope position of the surface outcrop of the front (Drinkwater et al. 1994; Loder et al. 1998). As compared with the position of the foot of the front, the location of the surface outcrop of the shelfbreak front can be quite variable both temporally and geographically. Drinkwater et al. (1994) calculated the mean surface position of the shelfbreak front (they refer to it as the shelf/slope front) from 20 years of sea surface temperature maps using satellite thermal imagery. They found that the surface outcrop of the shelfbreak front resides well seaward of the shelf break along the Scotian shelf. Upstream and downstream of this position, the surface outcrop lies closer to the shelf break (Lazier 1982;

Drinkwater et al. 1994). This is consistent with our climatology as well (see the salinity sections in Fig. 4b). Loder et al. (1998) pointed out the same trend using surface salinity. However, as our results indicate, it can be misleading to use the surface outcrop as an indicator of the position of the main front. This is corroborated by Pickart et al. (1999, e.g., their Fig. 12), who constructed average hydrographic fields across the shelf break at 50°W showing that a near-surface layer of low salinity water (with salinities as low as 34 psu) extends up to 100 km seaward of the deep expression of the shelfbreak front. In fact, the tongue of surface-trapped low salinity water outcrops into the region of eastward flow in the slopewater jet—completely outside of the region of equatorward flow. This suggests that the surface front, at least at this location, is actually separated from the bulk of the jet by a region of minimal horizontal gradients. For this reason, we suggest that the shelf/slope front discussed by Drinkwater et al. (1994) should be referred to, instead, as the surface shelf/slope front and not necessarily be considered an indicator of the position of the shelfbreak jet.

Our study is focused on the climatological mean state of the shelfbreak system during the summer season in the 1990s. It is important to note that the shelfbreak frontal system is forced both seasonally and interannually by various factors—including air–sea fluxes, freshwater discharge, wind stress, and ice coverage—all of which vary geographically. Interannual variability of the shelfbreak system has been documented in particular regions, though the underlying reasons for the long-term changes are not well understood. One particularly intriguing interannual mode involves a "flooding" of cold/fresh water through (at least parts of) the system (Worthington 1964; Petrie and Drinkwater 1993; Marsh et al. 1999). An extreme example of this occurred in the late 1800s when a portion of the U.S.–Canadian eastern seaboard cooled and freshened, resulting in a mass killing of tilefish (Marsh et al. 1999). Drinkwater et al. (2002) has documented a similar event that occurred in 1997 (although it was smaller in amplitude), relating it to an increase in transport of the Labrador Current. Various investigators have argued that the large-scale atmospheric forcing associated with the North Atlantic Oscillation is responsible for such interannual fluctuations, but this is not obvious (e.g., Pickart et al. 1999). Overall, cold/fresh Labrador Current water was only observed in the upper 200–400 m west of the Laurentian Channel a single time during the 1990s (our study period). During the remainder of the time the water along the Scotian shelf was actually warmer than average (similar to conditions in the 1950s and 1970s; Petrie and Drinkwater 1993).

Seasonal heating is a major influence on the front, resulting in the development of a seasonal thermocline that caps the front, as we have seen here. The salinity structure of the front remains more constant year-round, although there is an annual cycle largely driven by coastal runoff and ice melt. For instance, an increase in runoff in early summer along the northern Labrador shelf sharpens the salinity front at the shelfbreak thereby increasing the speed and transport of the Labrador Current (Lazier and Wright 1993). By contrast, the speed and transport of currents along the Scotian shelf reach a maximum in winter and spring, coincident with the passage of the annual freshwater pulse from the Gulf of St. Lawrence (Loder et al. 2003). Linder and Gawarkiewicz (1998) suggest that the along-shelf advection of a seasonal pulse of freshwater in the Middle Atlantic Bight may displace the shelfbreak front seaward. Similarly, our results suggest that the distribution of properties in the shelfbreak front is influenced by input from freshwater sources on the shelf and by the seaward export of freshwater from the shelf break and upper slope, both of which are seasonally influenced. While we are not able to specifically address the question of freshwater transport using our climatology (which requires absolute velocity), it would be interesting to investigate the large-scale response of the shelfbreak system to seasonal forcing. For instance, one wonders if there are seasonal changes in the position and structure of the shelfbreak front and jet over the full the length of the current? If so, can these changes be explained by local or remote (advective) influences? This issue will be addressed in the future using the winter portion of the climatological data.

Acknowledgments. The authors gratefully acknowledge Steve Lentz and Glen Gawarkiewicz for providing insight that benefited the presentation of this work. We are also thankful to Terry McKee and Doug Gregory who were helpful in the early stages of working with the climatological database. This work was supported by the National Science Foundation under Grants OCE00-95261 (PF) and OCE-0450658 (RP).

APPENDIX

Synoptic Sections and the Standard Grid

a. Extracting synoptic sections

Extracting synoptic sections from the historical database is not a trivial task, based on the large amount of data contained in the climatology and its format. For example, the climatology contains cruise identifiers with every hydrographic profile, but these are not

unique. To get around this we first sorted the historical data by date and grouped stations with the same cruise identifiers into synoptic surveys. For our purposes, a synoptic survey is defined as a group of stations occupied within a 30-day period, a reasonable length of time for a modern-day cruise. With these time criteria we were able to objectively identify stations that were collected as part of a single cruise. Last, we examined each synoptic survey and manually assigned stations to individual sections. To confirm that the final set of sections were indeed synoptic we computed the elapsed time for each section. The histogram of times is sharply peaked at 1–2 days with a mean of roughly 3 days. Ninety percent of the sections were completed in less than one week.

b. The standard grid

1) TOPOGRAPHY

The first step in making the standard grid was to construct the representative (or average) bottom profile for each box. For this, we compared two high-resolution bathymetry products: the 2′ gridded elevations/bathymetry for the world (ETOPO2) derived from satellite altimetry and shipboard soundings (Smith and Sandwell 1997), and the General Bathymetric Chart of the Oceans (GEBCO) database (1997 version). In general, GEBCO was found to be more accurate over a larger portion of our domain than ETOPO2, particularly along the West Greenland shelf break. Unfortunately, the GEBCO bathymetry does not extend onto the shelf near Cape Farewell. Therefore, even though the BIO database encompasses this region, we begin our analysis slightly downstream of Cape Farewell, on the southwest coast of Greenland.

Using the digitized GEBCO bathymetry, we computed average bottom profiles for each of the regional boxes in the following way. First, the bathymetry data was transformed from a latitude–longitude reference frame to local Cartesian coordinates. Next, we computed the local gradient in bottom depth at each grid point and plotted the inverse of its magnitude relative to the water depth at each point $[(dH/dx)^{-1}$ vs H, where positive x is the downslope direction and H is the water depth]. Because we defined our regional boxes so that the bathymetry within each box was relatively well behaved, the vector gradients are all roughly oriented in the same, seaward, direction. The resulting bottom slope "scatterplot" was then low passed to obtain a single curve describing the bottom slope as a function of bottom depth. After negative or zero bottom slopes were flagged and dropped from the composite, the low-passed curve was integrated to obtain an average bottom profile for the box. To facilitate comparisons between regional boxes, the origin of the cross-slope axis was aligned with the shelf break for each box. The shelf break was objectively identified as the shorewardmost position along the composite bottom profile coinciding with a large change in slope and a local maximum in curvature.

2) PROJECTION ONTO STANDARD GRID

Once the composite bottom profile was determined for each regional box, individual sections could be mapped onto the standard grid by assigning a cross-stream position to the corresponding water depth of each hydrographic station. Several issues complicated this process. First, soundings are not archived in the BIO database. To determine water depths, we used the gridded GEBCO bathymetry to look up the water depth for each station based on its geographic position. The second issue complicating the gridding process was that, because the water depth of a station is used to determine its cross-shelf position, flat shelves, canyons, and isolated plateaus and basins lead to spurious mappings. In other words, there can only be one cross-shelf position associated with each water depth. To remedy this, the boundaries of the regional boxes were drawn to exclude obvious topographic anomalies such as canyons and banks. Stations falling within these regions were automatically excluded from the synoptic section. In addition, the water depths for a synoptic section obtained from the GEBCO database were also examined for reversing slopes before the stations were projected onto the standard grid. When slope reversals were found, the water depths of the surrounding stations in the section were used to interpolate a new water depth for the intermediate station. Measurements that were deeper than the interpolated water depth at the affected station were deleted.

Because the topography varies within a regional box relative to the composite bottom profile, the original station spacing of each synoptic section was altered when the section was mapped onto the standard grid. This will have the greatest effect on the calculation of thermal wind shears. We have quantified this effect by comparing the projected station spacing with the original station spacing for each of the regional boxes and for the domain as a whole. If it was determined that a mapped station was relocated too far away from its original cross-slope position, it was dropped from the section. The dominant effect of the projection is to compress (rather than expand) the station spacing, particularly inshore of the shelf break. A histogram of offsets over the entire domain is sharply peaked near zero (−1.8 km) but slightly skewed, with an average

value of −6 km, indicating that the stations are generally compressed by less than one-quarter of the original station spacing. We note that in some instances stations were offset by up to one-third of their original station spacing. While these offsets are significant, an examination of individual boxes indicates that the largest effects are found inshore of the shelf break, outside our region of interest. This is not surprising since our method requires that the reference bottom profile have nonzero slope on the shelf, even for regions with large, relatively flat shelves. Therefore, shelf stations that are originally widely spaced but have similar water depths are mapped onto a narrower portion of the composite bottom profile. At the shelf break and seaward, where the shelf break jet typically resides, the offsets are much smaller than those over the shelf.

c. *Gridding and quality control*

Before interpolating the hydrographic observations onto the final standard grid, we computed potential temperature (θ) and potential density (σ_θ, referenced to the sea surface) and removed density inversions for each profile. There were some stations that contained minimal observations in the vertical, and these were discarded. If a spurious mapping occurred or if a station was located near a topographic anomaly, it was also discarded. After these criteria were satisfied, full sections were examined and discarded if 1) the section did not cross the shelf break, having at least one station over the slope; 2) the section contained less than three stations; or 3) there was not enough horizontal resolution to make the gridding meaningful.

The grid spacing of the final grid was $dx = 5$ km and $dz = 10$ m. Since this is finer than the original station spacing, a Laplacian-spline objective interpolation scheme was used to interpolate the data. In a few cases the original station spacing was large enough that the interpolation was performed in two stages onto grids with progressively finer resolution. In our experience, this approach resulted in smoother fields and eliminated the artificial noise introduced by interpolating over large distances. For sections with significant variations in vertical resolution (i.e., high resolution near the surface and decreased resolution at depth), the interpolation was performed on the shallow and deep regions separately and then combined in the interpolation to the final grid. The gridded density sections were examined a final time for interpolation noise and inversions exceeding 0.002 (typical accuracy of a CTD). Smaller inversions were assumed to be equivalent to no stratification and were typically found at depths well below the frontal region.

REFERENCES

Baggesgaard-Rasumssen, and Jacobsen, 1930: Contributions to the hydrography of the waters around Greenland in the year 1925. *Medd. Fra Kommiss. Havundersogelser,* **2** (10), 1–24.

Beardsley, R. C., and C. N. Flagg, 1976: The water structure, mean currents, and shelf-water/slope-water front on the New England continental shelf. *Mem. Soc. Roy. Sci. Liege,* **6,** 209–225.

Brown, W. S., and R. C. Beardsley, 1978: Winter circulation in the western Gulf of Maine: Part 1. Cooling and water mass formation. *J. Phys. Oceanogr.,* **8,** 265–277.

Buch, E., 2000: A monograph on the physical oceanography of the Greenland Waters. Danish Meteorological Institute Scientific Rep. 00-12, Danish Meteorological Institute, Copenhagen, Denmark, 405 pp.

Chapman, D. C., 2000: Boundary layer control of buoyant coastal currents and the establishment of a shelfbreak front. *J. Phys. Oceanogr.,* **30,** 2941–2955.

——, and R. C. Beardsley, 1989: On the origin of shelf water in the Middle Atlantic Bight. *J. Phys. Oceanogr.,* **19,** 384–391.

——, and S. J. Lentz, 1994: Trapping of a coastal density front by the bottom boundary layer. *J. Phys. Oceanogr.,* **24,** 1464–1479.

Clarke, R. A., 1984: Transport through the Cape Farewell-Flemish Cap section. *Rapp. P.-v. Reunn. Cons. Int. Explor. Mer,* **185,** 120–130.

——, H. W. Hill, R. F. Reiniger, and B. A. Warren, 1980: Current system south and east of the Grand Banks of Newfoundland. *J. Phys. Oceanogr.,* **10,** 25–65.

Colbourne, E., B. deYoung, S. Narayanan, and J. Helbig, 1997: Comparison of hydrography and circulation on the Newfoundland Shelf during 1990-1993 with the long-term mean. *Can. J. Fish. Aquat. Sci.,* **54,** 68–80.

Csanady, G. T., and P. Hamilton, 1988: Circulation of slopewater. *Cont. Shelf Res.,* **8,** 565–624.

Cuny, J. P., B. Rhines, P. P. Niiler, and S. Bacon, 2002: Labrador Sea boundary currents and the fate of the Irminger Sea Water. *J. Phys. Oceanogr.,* **32,** 627–647.

Drinkwater, K. F., R. A. Myers, R. G. Pettipas, and T. L. Wright, 1994: Climatic data for the northwest Atlantic: The position of the shelf/slope front and the northern boundary of the Gulf Stream between 50W and 75W, 1973-1992. Canadian Data Report of Fisheries and Ocean Sciences, Rep. 125, 9 pp.

——, B. Petrie, and P. C. Smith, 2002: Hydrographic variability on the Scotian Shelf during the 1990s. NAFO SCR Doc. 02/42, Serial No. N4653, 16 pp.

Fischer, J., and F. A. Schott, 2002: Labrador Sea Water tracked by profiling floats—From the boundary current into the open North Atlantic. *J. Phys. Oceanogr.,* **32,** 573–584.

Fissel, D. B., G. J. Pierlot, and O. J. Byrne, 1989: CTD measurements beneath the Labrador pack-ice, March 1989 (preliminary results). Arctic Sciences Ltd., Dartmouth, NS, Canada, 27 pp.

Fratantoni, P. S., R. S. Pickart, D. J. Torres, and A. Scotti, 2001: Mean structure and dynamics of the shelfbreak jet in the Middle Atlantic Bight during fall and winter. *J. Phys. Oceanogr.,* **31,** 2135–2156.

Gatien, M. G., 1976: A study in the slope water region south of Halifax. *J. Fish. Res. Board Can.,* **33,** 2213–2217.

Gawarkiewicz, G., and D. C. Chapman, 1992: The role of stratification in the formation and maintenance of shelf-break fronts. *J. Phys. Oceanogr.,* **22,** 753–772.

Greenberg, D. A., and B. D. Petrie, 1988: The mean barotropic circulation on the Newfoundland shelf and slope. *J. Geophys. Res.,* **93,** 15 541–15 550.

Han, G., C. G. Hannah, J. W. Loder, and P. C. Smith, 1997: Seasonal variation of the three-dimensional mean circulation over the Scotian Shelf. *J. Geophys. Res.,* **102,** 1011–1025.

Hannah, C. G., J. W. Loder, and D. G. Wright, 1996: Seasonal variation of the baroclinic circulation in the Scotia-Maine region. *Buoyancy Effects on Coastal Dynamics,* D. G. Aubrey and C. T. Friedrichs, Eds., Coastal Estuarine Studies, Vol. 53, Amer. Geophys. Union, 7–29.

Helland-Hansen, B., 1934: The Sognefjord section: Oceanographic observations in the northernmost part of the North Sea and the southern part of the Norwegian Sea. *James Johnstone Memorial Volume,* University Press of Liverpool, 257–274.

Kearns, E. J., and H. T. Rossby, 1998: Historical position of the North Atlantic Current. *J. Geophys. Res.,* **103,** 15 509–15 524.

Khatiwala, S. P., R. G. Fairbanks, and R. W. Houghton, 1999: Freshwater sources to the coastal ocean off northeastern North America: Evidence from $H_2{}^{18}O/H_2{}^{16}O$. *J. Geophys. Res.,* **104** (C8), 18 241–18 256.

Lavender, K. L., R. E. Davis, and W. B. Owens, 2000: Mid-depth recirculation observed in the interior Labrador and Irminger Seas by direct velocity measurements. *Nature,* **407,** 66–69.

Lazier, J. R. N., 1973: The renewal of Labrador Sea Water. *Deep-Sea Res.,* **20,** 341–353.

——, 1980: Oceanographic conditions at ocean weather ship Bravo, 1964-1974. *Atmos.–Ocean,* **18,** 227–238.

——, 1982: Seasonal variability of temperature and salinity in the Labrador Current. *J. Mar. Res.,* **40** (Suppl.), 341–356.

——, 1994: Observations in the Northwest Corner of the North Atlantic Current. *J. Phys. Oceanogr.,* **24,** 1449–1463.

——, and D. G. Wright, 1993: Annual velocity variations in the Labrador Current. *J. Phys. Oceanogr.,* **23,** 659–678.

Linder, C. A., and G. Gawarkiewicz, 1998: A climatology of the shelfbreak front in the Middle Atlantic Bight. *J. Geophys. Res.,* **103,** 18 405–18 423.

Loder, J. W., B. Petrie, and G. Gawarkiewicz, 1998: The coastal ocean off northeastern North America: A large-scale view. *The Sea,* A. R. Robinson and K. H. Brink, Eds., Regional Studies and Syntheses, Vol. 11, Wiley, 105–133.

——, C. G. Hannah, B. D. Petrie, and E. A. Gonzalez, 2003: Hydrographic and transport variability on the Halifax section. *J. Geophys. Res.,* **108,** 8003, doi:10.1029/2001JC001267.

Marsh, R., B. Petrie, C. R. Weidman, R. R. Dickson, J. W. Loder, C. G. Hannah, K. Frank, and K. Drinkwater, 1999: The 1882 tilefish kill—A cold event in shelf waters off the northeastern United States? *Fish. Oceanogr.,* **8,** 39–49.

Mclellan, H. J., 1957: On the distinctness and origin of the slope water off the Scotian Shelf and its easterly flow south of the Grand Banks. *J. Fish. Res. Board Can.,* **14,** 213–239.

Mountain, D. G., 1974: Bering Sea Water on the North Alaskan Shelf. Ph.D. dissertation, University of Washington, 153 pp.

Petrie, B., and C. Anderson, 1983: Circulation on the Newfoundland continental shelf. *Atmos.–Ocean,* **21,** 207–226.

——, and K. Drinkwater, 1993: Temperature and salinity variability on the Scotian Shelf and in the Gulf of Maine 1945-1990. *J. Geophys. Res.,* **98,** 20 079–20 089.

——, and J. Buckley, 1996: Volume and freshwater transport of the Labrador Current in Flemish Pass. *J. Geophys. Res.,* **101,** 28 335–28 342.

——, B. Toulany, and C. Garrett, 1988: The transport of water, heat and salt through the Strait of Belle Isle. *Atmos.–Ocean,* **26,** 234–251.

——, K. Drinkwater, D. Gregory, R. Pettipas, and A. Sandstrom, 1996: Temperature and salinity atlas for the Scotia Shelf and the Gulf of Maine. Canadian Tech. Rep. of Hydrography and Ocean Sciences, 171 pp.

Pickart, R. S., 2004: Shelfbreak circulation in the Alaskan Beaufort Sea: Mean structure and variability. *J. Geophys. Res.,* **109,** C04024, doi:10.1029/2003JC001912.

——, T. K. McKee, D. J. Torres, and S. A. Harrington, 1999: Mean structure and interannual variability of the slopewater system south of Newfoundland. *J. Phys. Oceanogr.,* **29,** 2541–2558.

——, D. J. Torres, and R. A. Clarke, 2002: Hydrography of the Labrador Sea during active convection. *J. Phys. Oceanogr.,* **32,** 428–457.

——, ——, and P. S. Fratantoni, 2005: The East Greenland Spill Jet. *J. Phys. Oceanogr.,* **35,** 1037–1053.

Rasmussen, L. L., G. Gawarkiewicz, and W. B. Owens, 2005: Slope water, Gulf Stream, and seasonal influences on southern Mid-Atlantic Bight circulation during the fall-winter transition. *J. Geophys. Res.,* **110,** C02009, doi:10.1029/2004JC002311.

Reverdin, G., P. P. Niiler, and H. Valdimarsson, 2003: North Atlantic Ocean surface currents. *J. Geophys. Res.,* **108,** 3002, doi:10.1029/2001JC001020.

Reynaud, T. H., A. J. Weaver, and R. J. Greatbatch, 1995: Summer mean circulation of the northwestern Atlantic Ocean. *J. Geophys. Res.,* **100,** 779–816.

Rudels, B., E. Fahrbach, J. Meincke, G. Budeus, and P. Eriksson, 2002: The East Greenland Current and its contribution to the Denmark Strait overflow. *ICES J. Mar. Sci.,* **59,** 1133–1154.

Smith, E. H., F. M. Soule, and O. Mosby, 1937: The Marion and General Greene expeditions to Davis Strait and Labrador Sea under the direction of the U.S. Coast Guard, 1928/31/33/34/35. U.S. Coast Guard Bulletin 19 (part 2), Washington, DC, 259 pp.

Smith, W. H. F., and D. T. Sandwell, 1997: Global sea floor topography from satellite altimetry and ship depth soundings. *Science,* **277,** 1956–1962.

Worthington, L. V., 1964: Anomalous conditions in the slope water area in 1959. *J. Fish. Res. Board Can.,* **21,** 327–333.

Wright, W. R., 1976: The limits of shelf water south of Cape Cod, 1941 to 1972. *J. Mar. Res.,* **34,** 1–14.